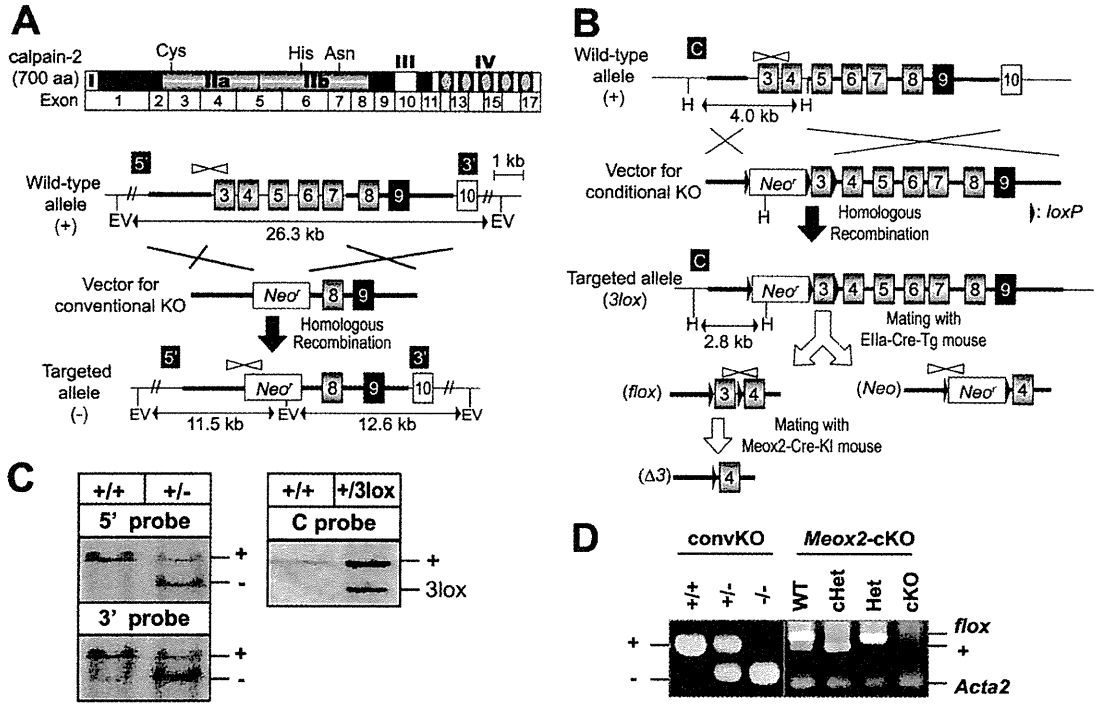

FIG. 1. Gene targeting of *Capn2* in mice. (A) Gene targeting for *Capn2* KO. Schematic representations of the domain structure of calpain-2 protein, the exon structure, the wild-type allele (+), the targeting vector for conventional *Capn2* KO, and the resultant targeted allele (−). Exons 3 to 7, including the catalytic triad (Cys105, His262, and Asn286 in protease domains IIa and IIb), were deleted in the targeted allele. The probe positions for Southern blotting (5′ and 3′ in black boxes), primer positions for *Capn2* KO PCR genotyping (white arrowheads), the homologous region with targeting vector (bold line), restriction enzyme EcoRV sites (EV), neomycin resistance gene cassette (Neo^r), and the expected sizes in Southern blotting are indicated. (B) Gene targeting for generation of the *Capn2* cKO and a second *Capn2* KO line. Schematic representations of the wild-type allele, the targeting vector for cKO, the targeted allele (*3lox*), and alleles deleted of *loxP*-flanked regions in *Cre*-transgenic mice (flox, Neo, and Δ3). By mating with *EIIa-Cre* transgenic mice (22), the *loxP*-flanked neomycin resistance gene cassette and exon 3 were removed from the (*3lox*) allele to generate the *Capn2* cKO line and another *Capn2* KO line, respectively. *Meox2-Cre* knock-in (KI) mice were mainly used for *Capn2* cKO analysis. The probe (C in black box) and restriction enzyme HindIII sites (H) for Southern blotting, primer positions for *Capn2* cKO PCR genotyping (black arrow), and *loxP* sequences (black arrowhead) are indicated. For PCR genotyping for the second *Capn2* KO line having the (Neo) allele, the same primers (see panel A) as for detection of the (−) allele were used. (C) Southern blotting to identify targeted embryonic stem cells. For the *Capn2* KO, the 11.5- and 12.6-kb genomic fragments from the (−) allele were detected with the 5′ and 3′ probes (black boxes in panel A), respectively. For the *Capn2* cKO, the 2.8-kb fragment from the (3lox) allele was detected with the C probe (black box in panel B). (D) PCR genotyping to identify mutant alleles. The left panel shows agarose gel electrophoresis of PCR products from $Capn2^{+/+}$, $Capn2^{+/-}$, and $Capn2^{-/-}$ fetuses. The right panel shows agarose gel electrophoresis of PCR products from $Meox2^{+/+}$ $Capn2^{+/flox}$ (WT), $Meox2^{Cre/+}$ $Capn2^{+/flox}$ (cHet), $Meox2^{+/+}$ $Capn2^{-/flox}$ (Het), and $Meox2^{Cre/+}$ $Capn2^{-/flox}$ (cKO) animals. In the cHet and cKO, the *flox* allele was deleted by Cre recombination.

regulated kinase (ERK) and protein kinase A has emerged as a candidate mechanism for regulating the activation status of calpain-2 (11, 28).

Another way to investigate the function of calpain is to manipulate the expression of calpastatin (*Cast*), which led us to generate *Cast* KO mice and transgenic (Tg) mice that overexpress calpastatin using the *Camk2a* promoter (17, 32). Both phenotypes were essentially normal in terms of their reproduction, development, growth, anatomy, and cognition, although the *Cast* KO mice exhibited modest abnormality in affective behavior (24). In contrast, calpastatin deficiency augmented excitotoxic neurodegeneration, which in turn was suppressed by calpastatin overexpression (17, 32). Thus, calpastatin appeared to play a more significant role under pathological rather than physiological conditions.

In summary, recent reverse genetic studies have highlighted the potential physiological importance of calpain-2. Here, we independently generated conventional and conditional *Capn2* KO mice and found that *Capn2* deficiency does not affect embryonic survival at the preimplantation stage but rather induces cell death in placental trophoblasts at later stages, followed by cardiovascular defects. However, calpain has been known as an executer of cell death, these results suggest that both calpain-1 and -2 also have a role in cell survival signaling or maintenance.

MATERIALS AND METHODS

Generation and characterization of *Capn2* conventional and conditional KO mice. The 10-kb targeting region from introns 2 to 10 of mouse calpain-2 gene was subcloned by PCR using the primers 5′-GGGTTGTGGAGCACTGCACA CTTTGTAGTTTTCCGCTGCAACCATTTGCTGTTCTCC-3′ and 5′-CTTTG CATTTGCCAAGGGGTGGGGGCCAAAAGACAGGCAGTGTGGGAAGA TGGAGC-3′ with 129/SvEv mouse strain bacterial artificial chromosome as a template. For the *Capn2* KO, exons 3 to 7 were replaced with a neomycin resistance gene cassette with phosphoglycerate kinase promoter and polyadenyl-

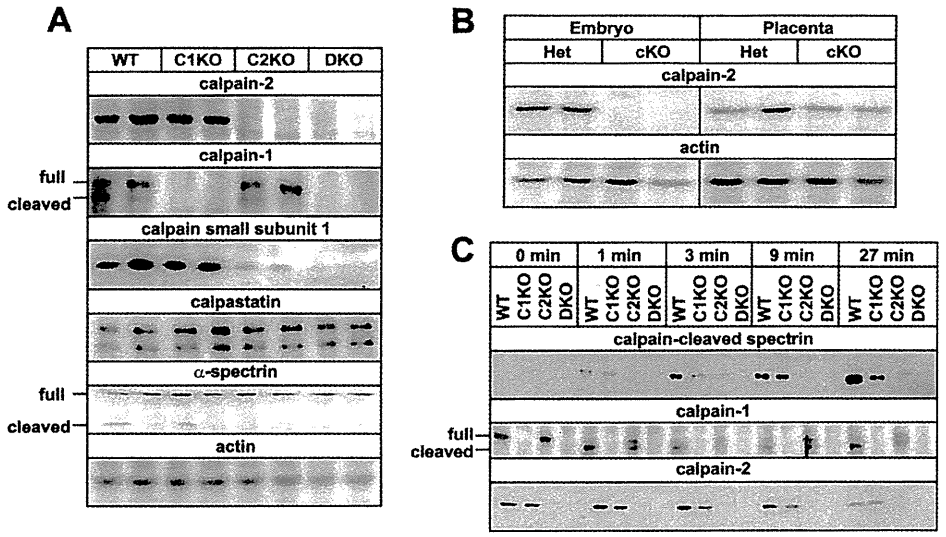

FIG. 2. Protein expressions and calpain activity. (A) Western blotting for *Capn2* conventional knockout fetuses. *Capn1*$^{+/+}$ *Capn2*$^{+/+}$ (WT), *Capn1*$^{-/-}$ *Capn2*$^{+/+}$ (C1KO), *Capn1*$^{+/+}$ *Capn2*$^{-/-}$ (C2KO), and *Capn1*$^{-/-}$ *Capn2*$^{-/-}$ (DKO) fetuses were analyzed at E10.5. Antibodies against calpain-2 domain IV, calpain-1 domain IV, calpain small subunit-1 domain VI, and calpastatin C terminus peptide were used. Using anti-calpain-1 antibody, the N-terminally autocleaved form was detected. (B) Western blotting for *Capn2* cKO from fetuses and placentas. E13.5 placentas from Het (*Meox2*$^{+/+}$ *Capn2*$^{-/flox}$) and cKO (*Meox2*$^{Cre/+}$ *Capn2*$^{-/flox}$) mice were analyzed. (C) Calpain activation assay. Calcium ion was added to brain homogenates from 3-month-old *Meox2*$^{+/+}$ *Capn1*$^{+/+}$ *Capn2*$^{+/+}$ (WT), *Meox2*$^{+/+}$ *Capn1*$^{-/-}$ *Capn2*$^{+/+}$ (C1KO), *Meox2*$^{Cre/+}$ *Capn1*$^{+/+}$ *Capn2*$^{-/flox}$ (C2cKO), and *Meox2*$^{Cre/+}$ *Capn1*$^{-/-}$ *Capn2*$^{-/flox}$ (cDKO) mice and then incubated for 0, 1, 3, 9, or 27 min at 30°C. The cleavage form of calpain-1 but not calpain-2 was detected.

ation regions to disrupt the catalytic triad of Cys105, His262, and Asn286 and make a frameshift mutation. For the *Capn2* conditional KO (cKO), exon 3 was flanked between a *loxP* sequence and a *loxP*-flanked neomycin resistance gene cassette. The targeting vectors were linearized and transfected by electroporation into embryonic stem cells derived from the 129 SvEv mouse strain.

After G418 treatment for the selection of the neomycin resistance gene-introduced clones, Southern blotting was performed to identify targeted clones using *Capn2*-specific probes, which were generated by genomic PCR using the primers 5′-TTGGAAGTCTGACAGCCAATAAAGC-3′ and 5′-TGAAGCCA GACCTGGCTTACAGTATTCC-3′ for the 5′ probe, the primers 5′-TCCTGA GATTTATACTGTGCCAGTGG-3′ and 5′-TTTAGATGGAGTGCTACTGA CAGAGG-3′ for the 3′ probe, and the primers 5′-CCCAGGTTTGGACTCAG AGACTG-3′ and 5′-TCTACATTGCATCTATGAAGATGTG-3′ for the C probe. Identified embryonic stem clones were microinjected into C57BL/6J blastocysts.

For embryonic analysis, noon of the day when a vaginal plug was recorded was considered to represent E0.5. To identify *Capn2* KOs, PCR genotyping was carried out using the three primers 5′-GAGAGTTCTGAGTTTCTCAGAGAA CGAACC-3′, 5′-AACTCCACGCCGTTCGGATGG-3′, and 5′-TGCGAGGCC AGAGGCCACTTGTGTAGC-3′. For *Capn2* cKOs, the 5′-GCTTGGCTTGCT CCTACACTCC-3′ and 5′-GCTCATCTGTGTCTCCAAAGCC-3′ primers were used with the *Acta2* primers 5′-GACAGGATGCAGAAGGAGAT-3′ and 5′-TTGCTGATCCACATCTGCTG-3′. For *Cre*-expressing mice, the 5′-CGCA GAACCTGAAGATGTTC-3′ and 5′-CGAAATCAGTGCGTTCGAAC-3′ primers were used with the *Gapdh* primers 5′-ACCACAGTCCATGCCATCA C-3′ and 5′-TCCACCACCCTGTTGCTG-3′. *EIIa*-, *Meox2*-, and *Tek-Cre* expressing mice (stock numbers 003724, 003755, and 004128, respectively) were provided by the Jackson Laboratory (20, 22, 33). Because Cre protein was expressed in germ cells under the influence of the *Meox2* promoter, *Meox2*$^{Cre/+}$ *Capn2*$^{+/-}$ males were mated to *Capn2*$^{flox/flox}$ females to generate *Capn2* cKO, Meox2$^{Cre/+}$ *Capn2*$^{-/flox}$ offspring. *Capn1* and *Cast* KO mice were as previously reported (3, 32).

Parental mice were backcrossed to C57BL/6J mice (Charles River Laboratories Japan, Inc.) over five generations. All animal experiments were carried out according to the RIKEN guidelines for animal experimentation.

Primary antibodies. Antibodies were generated against mouse calpain-2 and calpain-1 domain IV and calpain small subunit 1 domain VI, which were purified using an ImmunoPure Melon Gel IgG purification kit (Pierce) from the sera of rabbits immunized with each recombinant protein expressed in *Escherichia coli*. The anti-calpain cleaved spectrin and calpastatin antibodies were as previously generated (32). Other antibodies were purchased as indicated: α-spectrin (clone AA6; Biohit), β-actin (clone AC-15; Sigma-Aldrich), PECAM1 (clone MEC 13.3; BD Pharmingen), cytokeratin (Z0622; Dako), CD34 (MEC14.7; Abcam), smooth muscle actin (clone 1A4; Sigma-Aldrich), caspase-3 cleaved cytokeratin (M30; Roche), cleaved caspase-3 (antibody 9661; Cell Signaling Technology), cleaved caspase-8 (antibody 3259; BioVision), and cleaved caspase-9 (antibody 9504; Cell Signaling Technology).

Western blot analysis. Samples were homogenized in a 10-fold volume of 100 mM Tris-HCl (pH 7.5), 150 mM NaCl, 10 mM EDTA, 2 mM EGTA, 0.1% Triton X-100, and protease inhibitor cocktail (Roche). The techniques used for SDS-PAGE, Western blotting, immunoreactions, and detection with the ECL Advance Western blotting Kit (GE Healthcare) were as previously described (32).

For the calpain activity assay, brains were quickly frozen in liquid nitrogen and then homogenized in 20 mM Tris-HCl buffer (pH 7.5) containing 2 mM EDTA, 2 mM EGTA, 2 mM dithiothreitol, and 0.5 mg of Pefabloc (Roche)/ml, along with 0.3 μM aprotinin for serine protease inhibition, 40 μg of bestatin/ml for aminopeptidase inhibition, 1 μM pepstatin for aspartic protease inhibition, 100 nM epoxomicin for proteasome inhibition, 1× PhosSTOP phosphatase inhibitor cocktail (Roche), and 1% Triton X-100. After centrifugation at 10,000 × *g*, the supernatants were collected and incubated at 30°C after the addition of calcium chloride to a final concentration of 7 mM. The protein concentration of each sample was equalized by using BCA protein assay reagent (Pierce) to load equal amounts of samples.

Histochemistry. Mouse embryos were fixed in 4% paraformaldehyde in phosphate buffer (pH 7.3) for 24 h at 4°C. The embryos were then photographed with an Olympus SZX5 stereomicroscope. For slice staining, fixed embryos were dehydrated using an ethanol and xylene series and then embedded in paraffin blocks. The paraffin blocks were sliced at 8 μm in the case of embryos and at 4 μm for placentas. The sections were then rehydrated and stained with Mayer's hematoxylin and eosin solution (Wako Pure Chemical Industries). Immunohistochemical staining was performed by using a TSA-fluorescein system (Perkin-Elmer). To detect dead cells, an *in situ* cell death detection kit (Roche) was used with Hoechst 33342 counterstaining. Fluorescence images were acquired using a Nikon Eclipse E1000 fluorescence microscope or an Olympus FV300 confocal fluorescence microscope.

For whole-mount immunostaining, fetuses were dehydrated through a methanol series and bleached for 4 h in 5% H_2O_2 in methanol. After rehydration, the

TABLE 1. Genotypes of embryos from *Capn2*$^{+/-}$ intercrosses

Age (embryonic day)	No. of embryos with genotype[a]:		
	+/+	+/−	−/−
E12.5	4	7	7
E13.5	30	42	22
E14.5	20	36	16
E15.5	30	75	2*
E16.5	25	38	2*
Adult	68	146	0*

[a] *, $P < 0.001$ (chi-square test). The embryos at E12.5, E13.5, E14.5, and E16.5 were obtained from 2, 13, 10, 8, and 4 crosses, respectively.

fetuses were washed three times with 3% skim milk–0.1% Triton X-100 in phosphate-buffered saline (PBS-MT), followed by incubation with anti-PECAM1 antibody diluted in PBS-MT. After five washes with PBS-MT, the fetuses were incubated with horseradish peroxidase-conjugated anti-rat IgG antibody (GE Healthcare), washed five times with PBS-MT, and developed with 3,3-diaminobenzidine. The reaction was stopped by rinsing the fetuses three times in PBS.

DNA laddering assay. Placentas cleaned of maternal decidua were digested with proteinase K. After removal of the protein by phenol extraction, the DNAs were precipitated with sodium chloride-containing ethanol and dissolved in 10 mM Tris-HCl (pH 8.0) and 1 mM EDTA. Then, 10 μg of DNA and 200-bp ladder marker (TaKaRa) were loaded onto a 2% agarose gel. The loaded DNA was quantified by determining the absorbance at 260 nm.

RESULTS

Generation and characterization of conventional and conditional *Capn2* knockout mice together with *Capn1 Capn2* DKO mice. To generate conventional and conditional KO mice, we designed targeting vectors for homologous recombination in embryonic stem cells to disrupt the catalytic triad region in *Capn2*, i.e., exons 3 to 7 for the KO and exon 3 for the cKO (Fig. 1A and B). We created fetal-specific cKO mice using Cre recombinase knock-in mice under the control of the *Meox2* promoter (33). *Capn1 Capn2* double KO (DKO) mice were generated by crossbreeding *Capn1* and the above *Capn2* KO mice (3). We confirmed the success of the gene targeting by Southern blotting, genomic PCR and Western blotting (Fig. 1C and D, Fig. 2A and B).

In the fetuses, calpain-2 appeared to be more abundant than

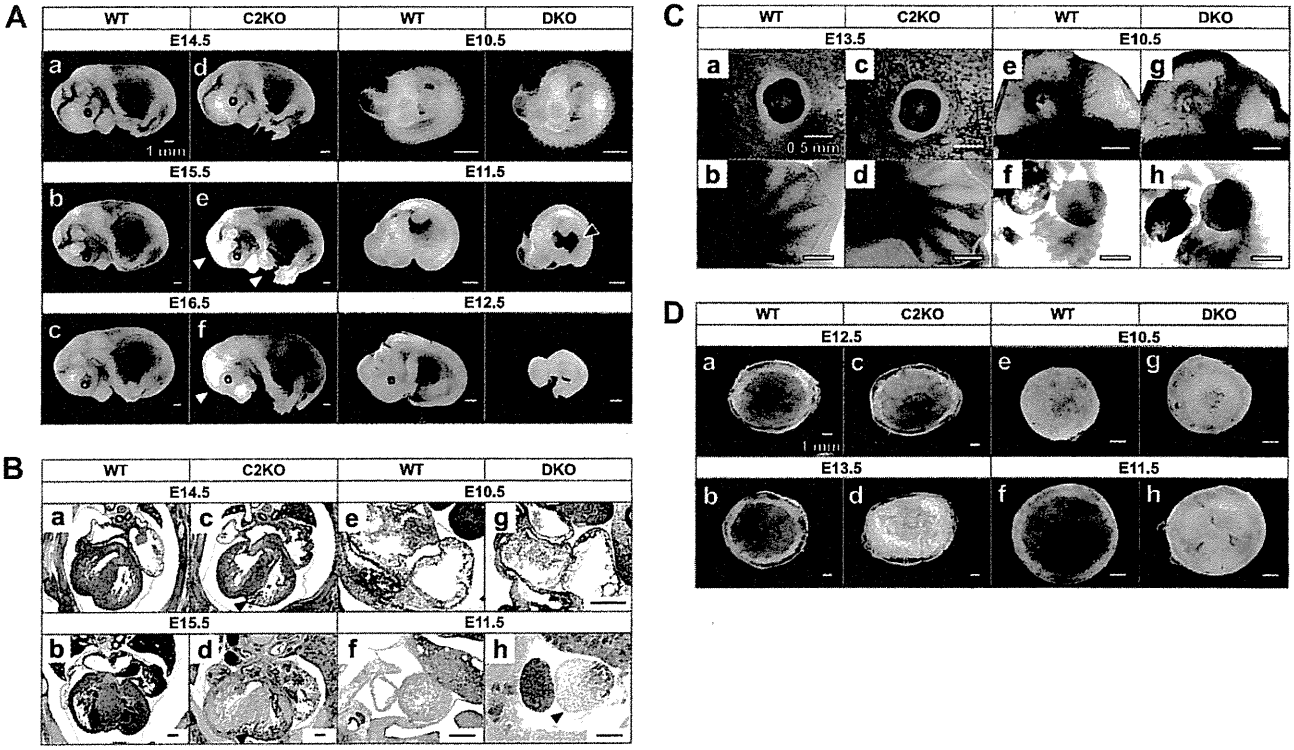

FIG. 3. *Capn2* knockout and *Capn1 Capn2* DKO embryos. (A) Appearance of mutant embryos. Wild-type (WT; a to c) and *Capn2*$^{-/-}$ embryos (C2KO; d to f) at E14.5 to E16.5 and wild-type (WT; g to i) and *Capn1*$^{-/-}$ *Capn2*$^{-/-}$ embryos (DKO; j to l) at E10.5 to E12.5 were photographed with a stereomicroscope. Peripheral vessels were diminished in six of 12 and all seven C2KO fetuses at E15.5 and E16.5, respectively (white arrowhead in panels e and f). Hepatic hemorrhages were detected in 6 of 11 DKO fetuses (black arrowhead in panel k). At E12.5 the all 14 DKO fetuses were absorbed (l). Tails were used for PCR genotyping. (B) Cardiac morphology. Transverse sections of WT (a and b) and C2KO (c and d) at E14.5 and E15.5 and sagittal sections of WT (e and f) and DKO (g and h) at E10.5 and E11.5 were stained with hematoxylin-eosin. The ventricular walls in C2KO and DKO were thinner than those of the WT (black arrowheads in panels c, d, and h). Cardiac abnormality was detected one of three and all three C2KO embryos at E14.5 and E15.5, respectively, and all three DKO embryos at E11.5. (C) Whole-mount immunostaining with anti-PECAM1 antibody. The eyes (a and c) and forelimbs (b and d) of the WT and C2KO at E13.5 and the head (e and g) and trunk (f and h) of the WT and DKO at E10.5 were visualized with diaminobenzidine after horseradish peroxidase-conjugated secondary antibody staining. We could not detected significant abnormality in all three C2KO and DKO embryos at this stage. (D) Appearance of placentas. Fetal sides of WT (a, b, e, and f), C2KO (c and d), and DKO (g and h) placentas were photographed with a stereomicroscope. Blood flow in the labyrinth was decreased in the C2KO and the DKO (d and h). We detected pale placentas (d and h) in four of 10 C2KO mice at E13.5 and all 10 DKO mice at E11.5.

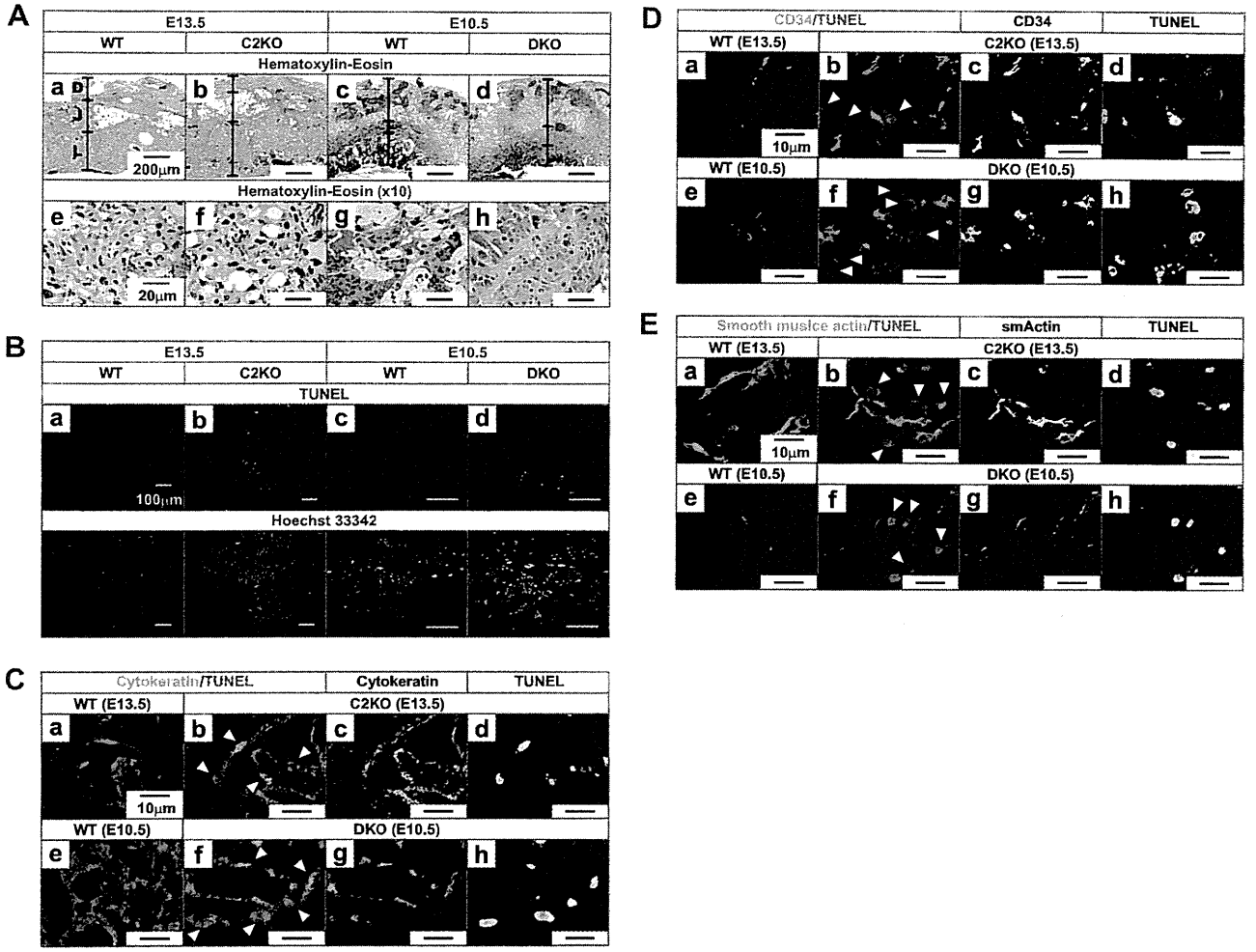

FIG. 4. Phenotype of a second *Capn2* knockout mouse generated using a different targeting vector. (A) Stereomicroscopy of wild-type (WT; a and b) and second *Capn2* KO (Neo/Neo; c and d) (Fig. 1B) fetuses and placentas. (B) Hematoxylin-eosin, *in situ* TUNEL, and Hoechst 33342 staining of wild-type (WT; a to c) and second *Capn2* KO (*Neo/Neo*; d to f) placentas.

calpain-1, with the calpain small subunit being almost nonexistent in *Capn2* KO mice but not in *Capn1* KO animals (Fig. 2A). Using an anti-α-spectrin antibody, a cleaved product of ~150 kDa was slightly detected. These calpain cleavage products do not seem to be generated under physiological conditions. Figure 2C shows that the *in vitro* calcium-dependent proteolytic activity in adult brain homogenates was slightly reduced in *Capn1* KO mice, almost fully abolished in *Capn2* cKO mice and completely absent in conditional DKO mice (cDKO), ($Meox2^{Cre/+}$ $Capn1^{-/-}$ $Capn2^{-/flox}$), a finding consistent with the quantity of calpain small subunit-1 present (Fig. 2A). These observations indicate that calpain-1 and -2 are primarily responsible for calcium-dependent calpain activity in the adult brain, with calpain-2 playing the major role, although calpain-1 alone exhibited appreciable proteolytic activity. We also confirmed similar proteolytic properties in mutant fetuses (data not shown).

Lethality of calpain knockout mice at various embryonic stages. Although the *Capn2* heterozygotes grew and bred normally, we were not able to obtain neonatal homozygous *Capn2* KO mice. To estimate the lethal stage, embryos from intercrossed heterozygous parental mice were collected and genotyped at different embryonic days (Table 1). Stereomicroscopic observations indicated failure of peripheral vessels in the limb and head regions from E15.5 in the *Capn2* KO mice (Fig. 3Ad to f). Another line of *Capn2* KO mice generated using a different targeting vector exhibited an identical phenotype (Fig. 4). Interestingly, this deteriorative phenotype was accelerated in DKO mice (Fig. 3Aj to l), with the fetuses dying ~3 days earlier (Table 2). This suggested additive nature of *Capn1* and *Capn2* deficiency *in vivo*, although *Capn1* deficiency alone appeared essentially harmless (3).

Because peripheral vessel failure could be caused by cardiovascular abnormality, we examined the cardiac region of the KO mice by hematoxylin-eosin staining. This analysis revealed cardiac disruption in the late but not the early stage of embryonic lethality. No significant abnormality, such as pericardial effusion or atrial enlargement (Fig. 3B), which is generally associated with defects in cardiac development (15, 38), was observed. Whole-mount immunostaining with

TABLE 2. Genotypes of embryos from *Capn1*$^{-/-}$ *Capn2*$^{+/-}$ intercrosses

Age (embryonic day)	No. of embryos with *Capn2* genotype[a]:		
	+/+	+/−	−/−
E9.5	11	19	13
E10.5	17	36	20
E11.5	28	49	15
E12.5	17	32	0*
E13.5	15	26	0*

[a] *, $P < 0.001$ (chi-square test). The embryos at E9.5, E10.5, E11.5, E12.5, and E13.5 were obtained from 7, 9, 12, 6, and 7 crosses, respectively.

anti-platelet endothelial cell adhesion molecule-1 (PECAM1) antibody detected no difference in vasculogenesis or angiogenesis between the control and mutant mice (Fig. 3C). Examination of other tissues revealed that the placental abnormalities arose prior to embryonic lethality (Fig. 3D); we observed paling of the placentas at E13.5 and at E11.5 in single *Capn2* (Fig. 3Dd) and DKO (Fig. 3Dh) mice, respectively.

Cell death in the placental labyrinth. Hematoxylin-eosin staining revealed normal development of the labyrinth and no abnormalities in the spongiotrophoblasts and trophoblast giant cells of the *Capn2* KO labyrinth but reduced development in the DKO labyrinth (Fig. 5A and Fig. 6C). *In situ* terminal deoxynucleotidyltransferase-mediated dUTP nick-end labeling (TUNEL) staining detected cell death with DNA fragmentation selectively in the mutant labyrinthine region (Fig. 5B). The TUNEL-positive cells were identified as trophoblasts which could be immunostained with anticytokeratin antibody (Fig. 5C). We could not detect any developmental abnormality in either the endothelium or the smooth muscle stained with

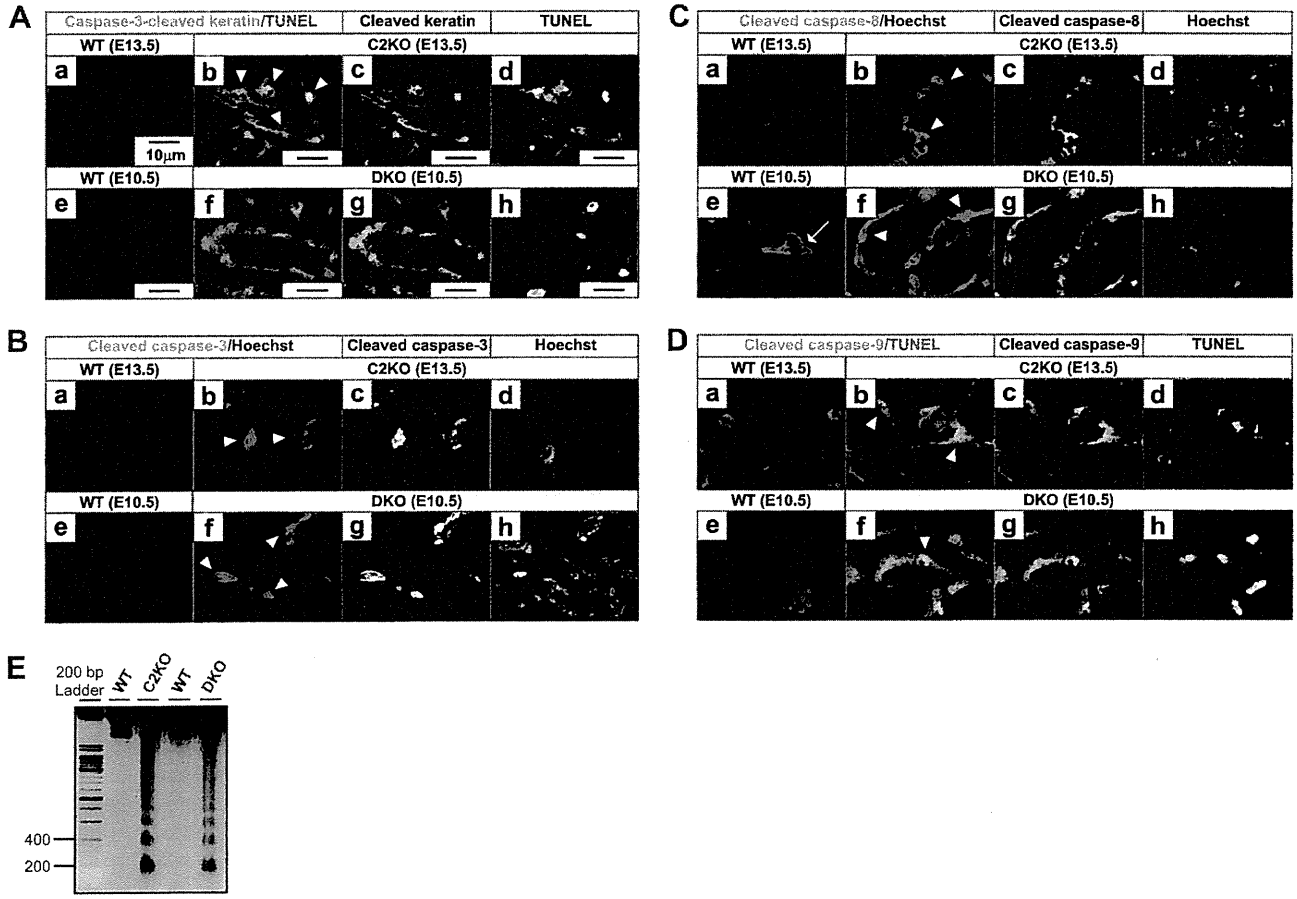

FIG. 5. Cell death in placental trophoblasts. (A) Hematoxylin-eosin staining of placental slices. (a to d) Three-layer structure formed by decidua (D), junctional zone (J; containing spongiotrophoblasts and giant cells), and labyrinth (L) is indicated. No growth abnormality of junctional zone were detected in the C2KO (b) or the DKO (d) (see Fig. 6) mice. Panels e to h are 10-fold-magnified images of the labyrinthine region. Severe developmental abnormalities were detected in the DKO (h) but not in the C2KO (f) mice. (B) *In situ* TUNEL and Hoechst 33342 double staining. TUNEL signals were detected specifically in the labyrinthine region of the C2KO and the DKO placentas (b and d). TUNEL-positive cells in the labyrinth were detected in 3 of 10 and 7 of 10 C2KO placentas at E13.5 and E14.5 and in 5 of 10 and all 10 DKO placentas at E10.5 and E11.5, respectively. (C) Double staining with *in situ* TUNEL and anticytokeratin antibody. TUNEL-positive cells in the C2KO and DKO mice (red in panels b and f, arrowheads) were costained with anticytokeratin antibody, a trophoblast marker (green). The images were acquired by confocal fluorescence microscopy. (D) Double staining with *in situ* TUNEL and anti-CD34 antibody. TUNEL-positive cells in the C2KO and DKO (red in panels b and f, arrowheads) did not costain with anti-CD34 antibody, an endothelial marker (green). (E) Double staining with *in situ* TUNEL and anti-smooth muscle actin antibody. TUNEL-positive cells in the C2KO and DKO (red in panels b and f, arrowheads) did not costain with anti-smooth muscle actin antibody, a blood vessel muscle marker (green).

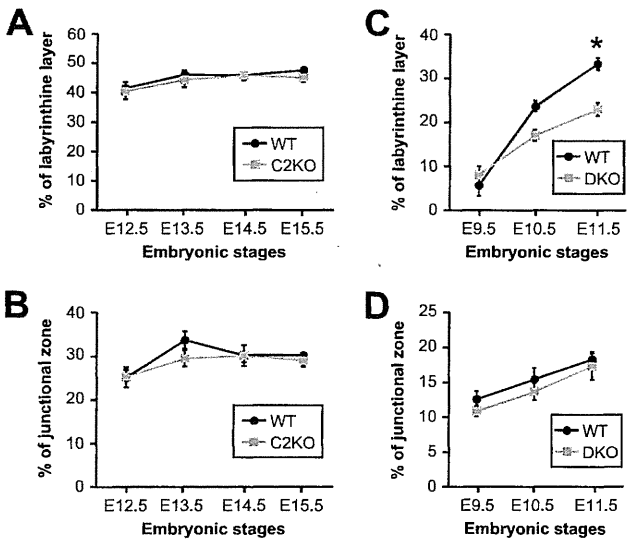

FIG. 6. Proportion of labyrinthine and junctional zones in *Capn2*$^{-/-}$ and *Capn1*$^{-/-}$ *Capn2*$^{-/-}$ placentas. (A and B) Proportion of labyrinthine and junctional zones of wild-type (WT) and *Capn2*$^{-/-}$ (C2KO) placentas. (C and D) Proportion of labyrinthine and junctional zones of WT and *Capn1*$^{-/-}$ *Capn2*$^{-/-}$ (DKO) placentas. Proportion of labyrinthine and junctional zones were quantified by measuring the length of each layer. Error bars indicate ± the standard errors of the mean. *, $P < 0.01$ (Tukey-Kramer test, $n = 8$ to 10 for each genotype and developmental stage).

anti-CD34 and smooth muscle actin antibodies, respectively (Fig. 5D and E).

Apoptosis-like cell death accompanying hyperactivation of caspases and DNA laddering. In an effort to identify the mechanism of cell death, we investigated the activation of caspases, well-known executors of apoptosis. Caspase-3, a death effector, was activated in *Capn2* KO and DKO trophoblasts (Fig. 7A and B). The activation of initiator caspases, caspase-8 and -9, remained in larger trophoblasts in both mutants, whereas wild-type labyrinth showed marginal activity (Fig. 7C and D). We also detected DNA fragmentation with a laddering pattern, a phenomenon that is typical of apoptosis (Fig. 7E). These results indicate that the nature of the cell death in the *Capn2* KO and DKO mice can be classified as apoptosis involving caspase activation and DNA laddering.

Genetic rescue of the embryo in fetus-specific conditional calpain knockout mice and in *Capn2 Cast* DKO mice. To confirm that the observed placental dysfunction leads to fetal lethality, we generated *Capn2* cKO mice carrying *Meox2* promoter-driven *Cre*, which only express *Capn2* in extraembryonic tissues, and cDKO mice (*Meox2*$^{Cre/+}$ *Capn1*$^{-/-}$ *Capn2*$^{-/flox}$). Nearly half of the *Capn2* cKO and cDKO mice survived to adulthood (Table 3). This observation indicates that the expression of calpain in the placenta is essential for normal development of the embryo. We also generated DKO mice deficient in *Capn2* and the calpastatin gene, *Cast*, to examine whether the presence or absence of this calpain inhibitor protein plays a role in embryogenesis. The *Capn2 Cast* DKO mice also appeared to lack any significant abnormality, although the probability of survival was ca. 50% lower than expected (Table 2C). In contrast, a deficiency in *Calpn1 Capn2 Cast* in triple-KO mice resulted in embryonic lethality at E11.5 (Table 4 and Fig. 8). The outcomes of multiple-crossbreeding among the *Capn1*, *Capn2*, and *Cast* KO mice are summarized in Table 5.

DISCUSSION

Our experimental results indicate that the calpain-calpastatin system plays an essential role in embryogenesis by regulating the survival of placental trophoblasts. Of the two calpain isozymes, calpain-2 appears to be the quantitatively predominant species in the embryo. Consistent with this, the phenotype that arises from calpain-2 deficiency is embryonic lethal, whereas that resulting from calpain-1 deficiency is essentially normal.

Two independent lines of *Capn2* KO mice that we generated using distinct targeting vectors consistently exhibited embryonic lethality at E15, in contrast to the previous report that *Capn2* KO embryos died at E2.5, prior to implantation (7). The reason for this discrepancy is unclear, but the extremely early death of the *Capn2* KO embryos in the latter case appears to be unnatural for two reasons. First, *Capns1* KO embryos which lack both calpain-1 and -2 die at E10.5, after implantation (2) and, second, *Capn1 Capn2* DKO mice die at E11.5 in a manner similar to *Capns1* KO mice. Consistent with the findings of Arthur et al. (2), our observations also indicate that the catalytic and regulatory subunits of calpain are both required for heterodimeric stability. Although more than 10 calpain isoforms have been identified in mammals (29), calpain-1 and -2 appear to account for essentially all of the calpain activity in the embryonic brain.

Although it is evident that calpain-2 plays a more important role than calpain-1 and calpastatin in embryogenesis, the latter two do influence the former. First, an additional lack of calpain-1 worsens the developmental phenotype of calpain-2 KO embryos. This additive effect of calpain-1 and -2 activities suggests that these isoforms share at least some functional redundancy, despite the difference in their *in vitro* calcium sensitivity. Second, it is notable that calpastatin deficiency partially rescued the lethal phenotype caused by calpain-2 deficiency. This is presumably because suppression of calpain-1 activity by calpastatin was removed in *Capn2* and *Cast* DKO embryos; consistent with this interpretation, triple calpain-1, calpain-2, and calpastatin deficiency resulted in the same embryonic lethality as that observed in the *Capn1 Capn2* DKO embryos.

These observations have profound implications for our understanding of the *in vivo* effect of the calpain-calpastatin system. First, both calpain-1 and -2 can be activated under physiological conditions in which calcium concentrations are generally in the submicromolar range, although they require micro- and millimolar concentrations of calcium, respectively, to exert an effect *in vitro*. Second, because these isozymes appear to share at least some functional redundancy, they are also likely to possess similar substrate specificity *in vivo*. Third, although calpastatin is known to bind and inhibit to calpain-1 and -2 in a calcium-dependent manner *in vitro* (13, 23, 37), the calpain-calpastatin interaction takes place under physiological conditions and, finally, autolysis of the regulatory domain in calpain-2 is unlikely to play a major role in the activation

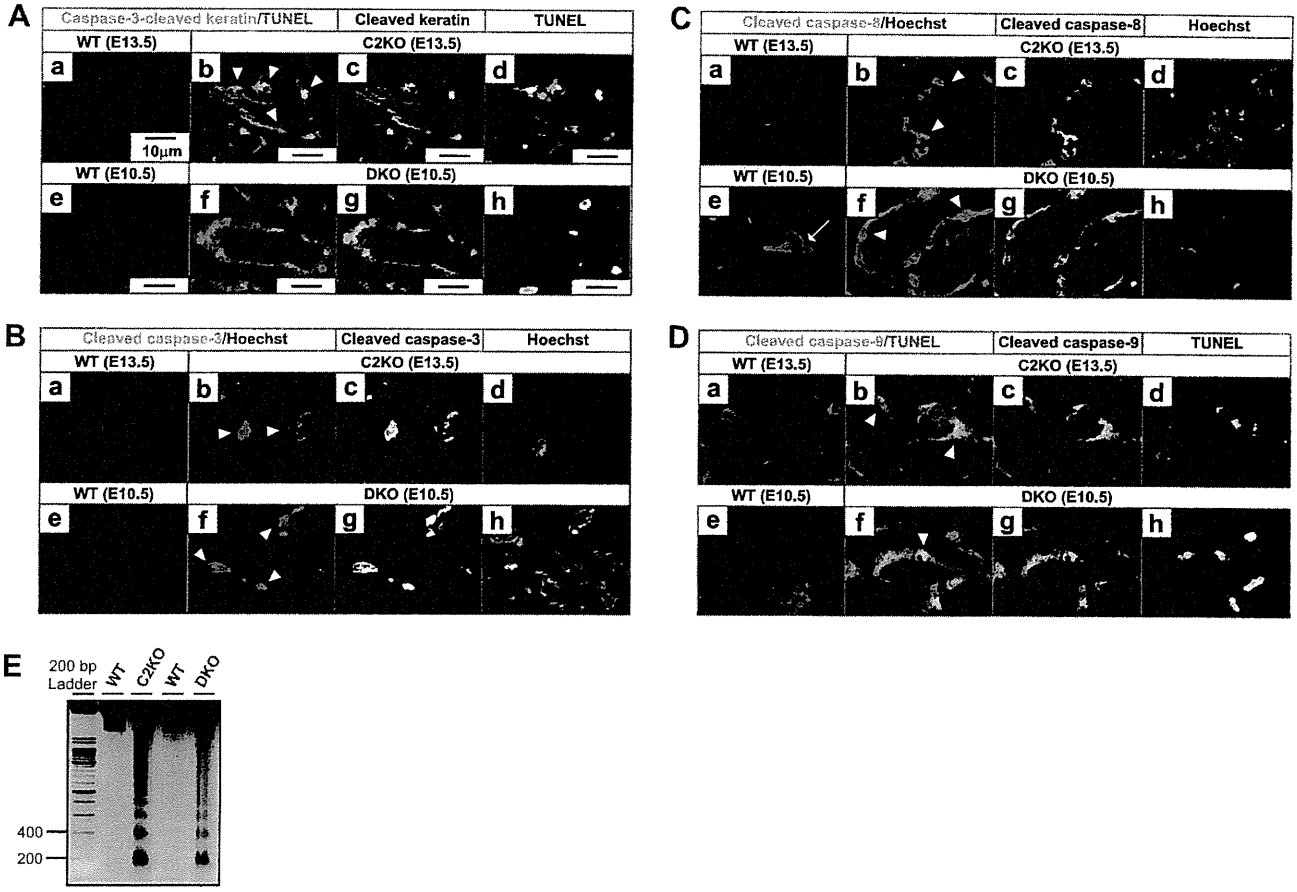

FIG. 7. Immunohistochemical study for caspase activation and apoptotic DNA fragmentation. (A) Double staining with anti-caspase-3-cleaved cytokeratin antibody and *in situ* TUNEL. Cells costained for anti-caspase-3-cleaved cytokeratin (green) and TUNEL (red) are indicated by the arrowheads (b and f). Panels a, b, e, and f represent merged color images. Panels c, d, g, and h are corresponding gray-scale images. The images were acquired by confocal fluorescence microscopy. The caspase-3-cleaved cytokeratin-positive cells in labyrinth were increased in 5 of 10 and 5 of 10 C2KO placentas at E13.5 and E14.5 and in 6 of 10 and all 10 DKO placentas at E10.5 and E11.5, respectively. (B) Double staining with anti-cleaved caspase-3 antibody and Hoechst 33342. Anti-cleaved caspase-3 antibody-positive cells (green) are indicated by the arrowheads (b and f). The cleaved caspase-3-positive cells in labyrinth were increased in 5 of 10 and 4 of 10 C2KO placentas at E13.5 and E14.5 and in 3 of 10 and 9 of 10 DKO placentas at E10.5 and E11.5, respectively. (C) Double staining with anti-cleaved caspase-8 antibody and Hoechst 33342. Anti-cleaved caspase-8 antibody-positive cells (green) are indicated by the arrowheads (b and f). The arrow indicates the caspase-8 activation in an undifferentiated WT trophoblast (e). The cleaved caspase-8-positive cells in labyrinth were increased in 6 of 10 and 5 of 10 C2KO placentas at E13.5 and E14.5 and in 4 of 10 and all 10 DKO placentas at E10.5 and E11.5, respectively. (D) Double staining with anti-cleaved caspase-9 and *in situ* TUNEL cells costained for anti-cleaved caspase-9 (green) and TUNEL (red) are indicated by arrowheads (b and f). The cleaved caspase-9-positive cells in labyrinth were increased in 7 of 10 C2KO placentas at both E13.5 and E14.5 and in 6 of 10 and all 10 DKO placentas at E10.5 and E11.5, respectively. (E) Agarose gel electrophoresis of labyrinthine DNA from the WT and C2KO at E14.5 and from the WT and DKO at E12.5 for characterization of DNA fragmentation. The image stained with ethidium bromide under UV light was inverted.

TABLE 3. Genotypes of *Meox2 Capn2* and *Capn1 Capn2* conditional knockout embryos

Genotype	No. of embryos[a]:	
	Mating 1	Mating 2
WT	27	27
Het	16	17
cHet	36	27
cKO	13	14

[a] Mating 1: $Meox2^{Cre/+}$ $Capn2^{+/-}$ and $Capn2^{flox/flox}$. For mating 1, WT, Het, cHet, and cKO denote $Meox2^{+/+}$ $Capn2^{+/flox}$, $Meox2^{+/+}$ $Capn2^{-/flox}$, $Meox2^{Cre/+}$ $Capn2^{+/flox}$, and $Meox2^{Cre/+}$ $Capn2^{-/flox}$, respectively. The mice were obtained from 15 crosses. Mating 2: $Meox2^{Cre/+}$ $Capn1^{-/-}$ $Capn2^{+/-}$ and $Capn1^{-/-}$ $Capn2^{flox/flox}$. For mating 2, WT, Het, cHet, and cKO denote $Meox2^{+/+}$ $Capn1^{-/-}$ $Capn2^{+/flox}$, $Meox2^{+/+}$ $Capn1^{-/-}$ $Capn2^{-/flox}$, $Meox2^{Cre/+}$ $Capn1^{-/-}$ $Capn2^{+/flox}$, and $Meox2^{Cre/+}$ $Capn1^{-/-}$ $Capn2^{-/flox}$, respectively. The mice were obtained from 16 crosses.

process because the catalytic subunit of calpain-2, unlike that of calpain-1, does not undergo autolysis for its activation (27).

The downstream events that follow calpain-2 activation appear to involve inactivation of caspase-3, -8, and -9. Caspase-8 is known to contribute to the fusion of cytotrophoblasts into syncytiotrophoblasts without cell death (4). However, calpain appears not to mediate placental trophoblast fusion, calpain inhibitors can suppress hCGβ (human chorionic gonadotropin beta subunit) secretion in placental culture (10). On the contrary, upregulation of calpain-1 in human decidua was suggested the relationship with recurrent miscarriage (21). Considering these results, control of calpain activation seems to be a key for proper embryonic development. To elucidate these

TABLE 4. Genotypes of *Capn1 Capn2* and *Cast Capn1 Capn2* knockout mice and *Tek Capn1 Capn2* conditional knockout mice

Genotype (1-month-old mice)	Cross (no. of crosses)	No. of mice with genotype:		
		+/+	+/−	−/−
Capn2	$Cast^{-/-}$ $Capn2^{+/-}$ (15)	37	52	14
	$Cast^{-/-}$ $Capn1^{-/-}$ $Capn2^{+/-}$ (6)	8	26	0[a]
Cre[b]	*Tek-Cre*$^{+/-}$ $Capn1^{-/-}$ $Capn2^{flox/flox}$ and $Capn1^{-/-}$ $Capn2^{flox/flox}$ (13)		41	42

[a] $P < 0.005$ (chi-square test).
[b] The *Tek-Cre*$^{+/-}$ $Capn1^{-/-}$ $Capn2^{flox/flox}$ mice did not show any significant abnormality for at least 1 year.

TABLE 5. Summary of the fetal phenotypes of calpain-calpastatin mutants

Genotype[a]			Phenotype	Source or reference
Capn1	*Capn2*	*Cast*		
WT	WT	WT	Normal	
KO	WT	WT	Normal	3
WT	KO	WT	Lethal at E15.5	Fig. 3Ae
WT	WT	KO	Normal	32
KO	KO	WT	Lethal at E11.5	Fig. 3Ak
KO	WT	KO	Normal	Data not shown
WT	KO	KO	Normal	Table 4
KO	KO	KO	Lethal at E11.5	Fig. 8

[a] WT, wild type; KO, knockout.

phenomena, we should test reproductive capability and placental cell death using parental *Meox2 Capn2* cKO mice.

Several reports indicate that abnormalities in placental development may cause defects in the embryonic cardiovascular system (1, 12, 31). We have provided more conclusive evidence regarding the essential role of calpain in placental development using cKO and cDKO mice, in which calpain-2 expression is limited in the extraembryonic region by the *Meox2-Cre* transgene. Another cDKO mouse line under the control of *Tek-Cre* endothelium-specific deleter (20) survived to adulthood without significant abnormality (Table. 2E). This observation indicates that the cardiovascular phenotype was not caused by calpain deficiency in the blood vessels, of which endothelial cells are a major constituent. However, there is a possibility that other tissues other than those of placental trophoblasts are involved in embryonic lethality in *Meox2-Cre* induced cKO embryos because they still showed partial lethality.

These findings also have obstetric implications, given that labyrinthine trophoblasts play a critical role in the exchange of oxygen and nutrients between the maternal and embryonic circulations (25). Indeed, preeclampsia, a disease of human pregnancy, seems to be associated with cell death in the placenta (8, 19, 30). Despite the fact that a substantial number of human pregnancies fail as spontaneous abortions after implantation, the underlying mechanisms remain undetermined. The present study points to the possibility that calpain can act as a target for the prevention and treatment of preeclampsia and other maternal-embryonic diseases that accompany placental cell death.

Finally, there are still a number of questions that remain to be addressed. First, nothing is known about the postembryonic functions of calpain. Use of *Cre*-Tg mice under the control of various promoters should provide some insight regarding this. Second, the *in vivo* mechanism of calpain-1 and -2 activation has not yet been fully elucidated. The generation of multiple mutant mice deficient in or overexpressing components of the mitogen-activated protein kinase/extracellular signal-regulated kinase and calpain signaling systems may provide us with some additional clues. Third, we know nothing about the functional difference between calpain-1 and -2, although the present study indicates that these isozymes share at least some redundancy. Fourth, we do not yet have solely calpain-specific cell-permeable inhibitors, let alone an inhibitor that can distinguish between calpain-1 and -2. Such inhibitors would be extremely beneficial for both basic and clinical studies of the effects of calpain. Again, mutant mice and cells that lack or overexpress calpain-calpastatin system components would provide useful tools for screening inhibitors and possibly activators, with the determination of the three-dimensional structure of calpain (18), thereby generating an appreciable momentum for such efforts.

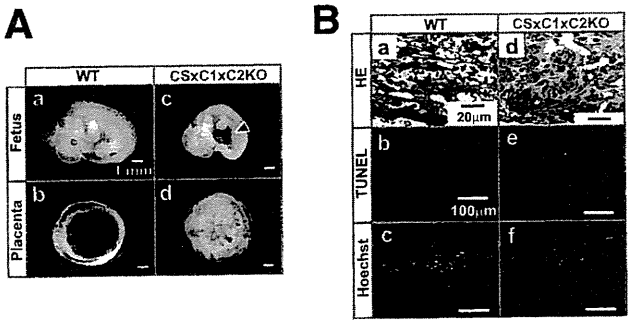

FIG. 8. Phenotype of the $Cast^{-/-}$ $Capn1^{-/-}$ $Capn2^{-/-}$ embryo. (A) Stereomicroscopy of wild-type (WT [a and b]) and $Cast^{-/-}$ $Capn1^{-/-}$ $Capn2^{-/-}$ (CS×C1×C2KO [c and d]) fetuses and placentas at E11.5. Hemorrhages were detected in the trunk region of the CS×C1×C2KO (arrowhead in panel c). (B) Hematoxylin-eosin, *in situ* TUNEL, and Hoechst 33342 staining of WT (a to c) and second CS×C1×C2KO (d to f) placentas.

ACKNOWLEDGMENTS

We acknowledge Mika Tanaka (RIKEN), Satoshi Tanaka (Tokyo University), and Yasuhiko Ozaki (Nagoya City University) for placental analysis, as well as Issei Komuro and Hiroshi Akazawa of Osaka University for cardiac diagnosis of mouse embryos. We also thank Masaki Kumai, Masanobu Kawatana, and Mayu Kawasaki for technical assistance.

This study was supported by research grants from the RIKEN Brain Science Institute and by Special Coordination Funds for Promoting Science and Technology from the Ministry of Education, Culture, Sports, Science, and Technology and the Ministry of Health, Labor, and Welfare of the Japanese Government.

REFERENCES

1. **Adams, R. H., et al.** 2000. Essential role of p38α MAP kinase in placental but not embryonic cardiovascular development. Mol. Cell **6**:109–116.
2. **Arthur, J. S., J. S. Elce, C. Hegadorn, K. Williams, and P. A. Greer.** 2000. Disruption of the murine calpain small subunit gene, *Capn4*: calpain is essential for embryonic development but not for cell growth and division. Mol. Cell. Biol. **20**:4474–4481.

3. **Azam, M., et al.** 2001. Disruption of the mouse μ-calpain gene reveals an essential role in platelet function. Mol. Cell. Biol. **21:**2213–2220.
4. **Black, S., et al.** 2004. Syncytial fusion of human trophoblast depends on caspase 8. Cell Death Differ. **11:**90–98.
5. **Carafoli, E., and M. Molinari.** 1998. Calpain: a protease in search of a function? Biochem. Biophys. Res. Commun. **247:**193–203.
6. **Croall, D. E., and G. N. DeMartino.** 1991. Calcium-activated neutral protease (calpain) system: structure, function, and regulation. Physiol. Rev. **71:**813–847.
7. **Dutt, P., et al.** 2006. m-Calpain is required for preimplantation embryonic development in mice. BMC Dev. Biol. **6:**3.
8. **Feinberg, B. B.** 2006. Preeclampsia: the death of Goliath. Am. J. Reprod. Immunol. **55:**84–98.
9. **Franco, S. J., and A. Huttenlocher.** 2005. Regulating cell migration: calpains make the cut. J. Cell Sci. **118:**3829–3838.
10. **Gauster, M., et al.** 2010. Caspases rather than calpains mediate remodeling of the fodrin skeleton during human placental trophoblast fusion. Cell Death Differ. **17:**336–345.
11. **Glading, A., P. Chang, D. A. Lauffenburger, and A. Wells.** 2001. Epidermal growth factor receptor activation of calpain is required for fibroblast motility and occurs via an ERK/MAP kinase signaling pathway. J. Biol. Chem. **275:** 2390–2398.
12. **Goll, D. E., V. F. Thompson, H. Li, W. Wei, and J. Cong.** 2003. The calpain system. Physiol. Rev. **83:**731–801.
13. **Hanna, R. A., R. L. Campbell, and P. L. Davies.** 2008. Calcium-bound structure of calpain and its mechanism of inhibition by calpastatin. Nature **456:**409–412.
14. **Hatano, N., Y. Mori, Oh-hora, et al.** 2003. Essential role for ERK2 mitogen-activated protein kinase in placental development. Genes Cells **8:**847–856.
15. **Hein, L., et al.** 1997. Overexpression of angiotensin AT1 receptor transgene in the mouse myocardium produces a lethal phenotype associated with myocyte hyperplasia and heart block. Proc. Natl. Acad. Sci. U. S. A. **94:**6391–6396.
16. **Hernandez, A. A., and W. R. Roush.** 2002. Recent advances in the synthesis, design and selection of cysteine protease inhibitors. Curr. Opin. Chem. Biol. **6:**459–465.
17. **Higuchi, M., et al.** 2005. Distinct mechanistic roles of calpain and caspase activation in neurodegeneration as revealed in mice overexpressing their specific inhibitors. J. Biol. Chem. **280:**15229–15237.
18. **Hosfield, C. M., J. S. Elce, P. L. Davies, and Z. Jia.** 1999. Crystal structure of calpain reveals the structural basis for Ca^{2+}-dependent protease activity and a novel mode of enzyme activation. EMBO J. **18:**6880–6889.
19. **Jurisicova, A., J. Detmar, and I. Caniggia.** 2005. Molecular mechanisms of trophoblast survival: from implantation to birth. Birth Defects Res. **75:**262–280.
20. **Koni, P. A., et al.** 2001. Conditional vascular cell adhesion molecule 1 deletion in mice: impaired lymphocyte migration to bone marrow. J. Exp. Med. **93:**741–754.
21. **Kumagai, K., et al.** 2008. Role of mu-calpain in human decidua for recurrent miscarriage. Am. J. Reprod. Immunol. **59:**339–346.
22. **Lakso, M., et al.** 1996. Efficient *in vivo* manipulation of mouse genomic sequences at the zygote stage. Proc. Natl. Acad. Sci. U. S. A. **93:**5860–5865.
23. **Moldoveanu, T., K. Gehring, and D. R. Green.** 2008. Concerted multi-pronged attack by calpastatin to occlude the catalytic cleft of heterodimeric calpains. Nature **456:**404–408.
24. **Nakajima, R., et al.** 2008. Comprehensive behavioral phenotyping of calpastatin-knockout mice. Mol. Brain. **1:**7.
25. **Rossant, J., and J. C. Cross.** 2001. Placental development: lessons from mouse mutants. Nat. Rev. Genet. **2:**538–548.
26. **Saido, T. C., H. Sorimachi, and K. Suzuki.** 1994. Calpain: new perspectives in molecular diversity and physiological-pathological involvement. FASEB J. **8:**814–822.
27. **Saido, T. C., et al.** 1994. Distinct kinetics of subunit autolysis in mammalian m-calpain activation. FEBS Lett. **346:**263–267.
28. **Shiraha, H., A. Glading, J. Chou, Z. Jia, and A. Wells.** 2002. Activation of m-calpain (calpain II) by epidermal growth factor is limited by protein kinase A phosphorylation of m-calpain. Mol. Cell. Biol. **22:**2716–2727.
29. **Sorimachi, H., and K. Suzuki.** 2001. The structure of calpain. J. Biochem. **129:**653–664.
30. **Straszewski-Chavez, S. L., V. M. Abrahams, and G. Mor.** 2005. The role of apoptosis in the regulation of trophoblast survival and differentiation during pregnancy. Endocrinol. Rev. **26:**877–897.
31. **Suzuki, K., and H. Sorimachi.** 1998. A novel aspect of calpain activation. FEBS Lett. **433:**1–4.
32. **Takano, J., et al.** 2005. Calpain mediates excitotoxic DNA fragmentation via mitochondrial pathways in adult brains: evidence from calpastatin mutant mice. J. Biol. Chem. **280:**16175–16184.
33. **Tallquist, M. D., and P. Soriano.** 2000. Epiblast-restricted Cre expression in MORE mice: a tool to distinguish embryonic versus extra-embryonic gene function. Genesis **26:**113–115.
34. **Wang, K. K. W., and P. W. Yuen.** 1999. Calpain: pharmacology and toxicology of calcium-dependent protease. Taylor and Francis, Philadelphia, PA.
35. **Wu, L., et al.** 2003. Extra-embryonic function of Rb is essential for embryonic development and viability. Nature **421:**942–947.
36. **Yamada, M., et al.** 2009. Inhibition of calpain increases LIS1 expression and partially rescues *in vivo* phenotypes in a mouse model of lissencephaly. Nat. Med. **15:**1202–1207.
37. **Yang, H. Q., H. Ma, E. Takano, M. Hatanaka, and M. Maki.** 1994. Analysis of calcium-dependent interaction between amino-terminal conserved region of calpastatin functional domain and calmodulin-like domain of μ-calpain large subunit. J. Biol. Chem. **269:**18977–18984.
38. **Yao, T. P., et al.** 1998. Gene dosage-dependent embryonic development and proliferation defects in mice lacking the transcriptional integrator p300. Cell **93:**361–372.
39. **Zatz, M., and A. Starling.** 2005. Calpains and disease. N. Engl. J. Med. **352:**2413–2423.

The FASEB Journal article fj.11-187740. Published online December 15, 2011.

The FASEB Journal • Research Communication

Mechanistic involvement of the calpain-calpastatin system in Alzheimer neuropathology

Makoto Higuchi,*,†,1,2 Nobuhisa Iwata,*,1 Yukio Matsuba,* Jiro Takano,* Takahiro Suemoto,* Jun Maeda,† Bin Ji,† Maiko Ono,‡ Matthias Staufenbiel,‡ Tetsuya Suhara,† and Takaomi C. Saido*,3

*Laboratory for Proteolytic Neuroscience, Rikagaku Kenkyūjo (RIKEN) Brain Science Institute, Wako, Saitama, Japan; †Molecular Imaging Center, National Institute of Radiological Sciences, Chiba, Chiba, Japan; and ‡Novartis Institute of Biomedical Research Basel, Basel, Switzerland

ABSTRACT **The mechanism by which amyloid-β peptide (Aβ) accumulation causes neurodegeneration in Alzheimer's disease (AD) remains unresolved. Given that Aβ perturbs calcium homeostasis in neurons, we investigated the possible involvement of calpain, a calcium-activated neutral protease. We first demonstrated close postsynaptic association of calpain activation with Aβ plaque formation in brains from both patients with AD and transgenic (Tg) mice overexpressing amyloid precursor protein (APP). Using a viral vector-based tracer, we then showed that axonal termini were dynamically misdirected to calpain activation-positive Aβ plaques. Consistently, cerebrospinal fluid from patients with AD contained a higher level of calpain-cleaved spectrin than that of controls. Genetic deficiency of calpastatin (CS), a calpain-specific inhibitor protein, augmented Aβ amyloidosis, tau phosphorylation, microgliosis, and somatodendritic dystrophy, and increased mortality in APP-Tg mice. In contrast, brain-specific CS overexpression had the opposite effect. These findings implicate that calpain activation plays a pivotal role in the Aβ-triggered pathological cascade, highlighting a target for pharmacological intervention in the treatment of AD.—Higuchi, M., Iwata, N., Matsuba, Y., Takano, J., Suemoto, T., Maeda, J., Ji, B., Ono, M., Staufenbiel, M., Suhara, T., Saido, T. C. Mechanistic involvement of the calpain-calpastatin system in Alzheimer neuropathology. *FASEB J.* 26, 000–000 (2012). www.fasebj.org**

Key Words: amyloid precursor protein · APP · amyloid β peptide · Aβ · humans · mice

EXTENSIVE PATHOLOGICAL, HUMAN genetic, molecular biological, and reverse genetic studies have established that abnormal accumulation of amyloid-β peptide (Aβ) in brain triggers the neuropathological cascade characteristic of Alzheimer's disease (AD) development (1–3). However, the molecular mechanisms underlying the subsequent hallmark processes of the disease, such as tauopathy and neurodegeneration, remain largely unknown (3–4).

Because perturbation of calcium homeostasis has been implicated as a common mechanism in diverse forms of brain injury (5–7) and because overload of amyloidogenic molecules, such as Aβ and tau, elevates intracellular calcium concentration (8–12), we hypothesized that the calcium-dependent cysteine protease, calpain (EC 3.4.22.17), could be involved in the loss of neuronal integrity in the AD brain. Consistently, cytoskeletal components in neurons, such as tau, microtubule-associated protein 2 (MAP2), neurofilaments, and spectrin, are predisposed to enzymatic cleavage by activated calpain (5, 13), and increased levels of calpain are frequently found to overlap with senile plaques and

Abbreviations: 136kf, calpain-cleaved amino-terminal 136-kDa fragment of α-spectrin; 150kf, calpain-cleaved carboxyl-terminal 150-kDa fragment of α-spectrin; Aβ, amyloid β peptide; AD, Alzheimer's disease; APP, amyloid precursor protein; BP_{ND}, nondisplaceable binding potential; Clact32, caspase-cleaved amino-terminal 32-kDa fragment of actin; CS, calpastatin; CSF, cerebrospinal fluid; CS-KO, calpastatin-knockout; dTg, double transgenic; Erk, extracellular signal-regulated kinase; FSB, 1-fluoro-2,5-bis(3-carboxy-4-hydroxystyryl)benzene; GABA, γ-aminobutyric acid; GAP43, growth-associated protein 43; MAP2, microtubule-associated protein 2; MAPK, 1,2-mitogen-activated protein kinase; MR, magnetic resonance; NFH, neurofilament high-molecular-weight subunit; NMDA, *N*-methyl-D-aspartate; PB, phosphate buffer; PET, positron emission tomography; PIB, Pittsburgh compound-B; rAAV-NEP-MUT, recombinant adeno-associated viral vector expressing mutant, nonfunctioning human neprilysin; SNAP-25, synaptosomal-associated protein 25; SV2A, synaptic vesicle glycoprotein 2A; PSD-95, postsynaptic density-95 protein; Tg, transgenic; TSA, tyramide signal amplification; TUNEL, terminal deoxynucleotidyl transferase deoxyuridine triphosphate nick end labeling; WT, wild-type.

[1] These authors contributed equally to this work.

[2] Current address: Molecular Imaging Center, National Institute of Radiological Sciences, 4-9-1 Anagawa, Inage-ku, Chiba, Chiba 263-8555, Japan.

[3] Correspondence: Laboratory for Proteolytic Neuroscience, RIKEN Brain Science Institute, 2-1 Hirosawa, Wako, Saitama 351-0198, Japan. E-mail: saido@brain.riken.jp

doi: 10.1096/fj.11-187740

This article includes supplemental data. Please visit *http://www.fasebj.org* to obtain this information.

neurofibrillary tangles in autopsied brains from patients with AD (14, 15).

Calpain can be characterized by its molecular diversity and structural complexity. The calpain family comprises at least 6 isozymes in mammals; μ-calpain and m-calpain, which are known to be proteolytically active in the brain, exist as heterodimers comprising distinct large subunits and identical small subunits (5), making it difficult to relevantly manipulate *in vivo* calpain activity by genetically engineering calpain genes. Although a number of commercially available synthetic "calpain inhibitors" have been described, none, to our knowledge, are truly specific to calpain, as they also inhibit other cysteine proteases, such as cathepsins B, H, L, K, and S (5–16). The only calpain-specific inhibitor reported thus far is a cytoplasmic protein, calpastatin (CS; ref. 5). The affinity of CS for activated calpain is extremely high, with the K_i value for m-calpain being estimated as 10 nM in one study (5). CS deficiency appears to cause no abnormality in reproduction, development, longevity, or behavior, with no detectable calpain activation occurring under normal conditions (ref. 17 and unpublished results; see also Results). In contrast, kainate-induced neurotoxicity results in up- and down-regulation of calpain-catalyzed proteolysis, as well as subsequent degenerative changes in CS-knockout (CS-KO) and CS-overexpressing mutant mice, respectively (17, 18), indicating that CS functions as a decelerator of calpain under essentially pathological conditions. Because CS inhibits μ-calpain and m-calpain in an identical and stoichiometric manner and because calpain inhibition is the only function of CS thus far identified (5), genetically engineered mice lacking or overexpressing CS provide useful models with which to examine the involvement of the calpain-CS system in a given disorder.

In this study, we first investigated calpain activation in brains from patients with AD and amyloid precursor protein–transgenic (APP-Tg) mice. We then analyzed the effects of CS deficiency and overexpression on the pathological phenotypes in the Tg animals, *i.e.*, cytoskeletal proteolysis, Aβ deposition, tau phosphorylation, microglial activation, and neurodegeneration, in order to determine whether a causal relationship could be established. The effect of calpain hypoactivation and hyperactivation appeared to be quite specific to AD pathology, because an independent attempt to induce alcoholic neurodegeneration under possibly the harshest conditions, *i.e.*, replacement of the entire drinking water by 30% ethanol for 10 wk, exerted no effect on the CS-KO mice (unpublished results), despite the fact that ethanol potentiates calcium influx *via* type A γ-aminobutyric acid ($GABA_A$) receptor (19).

MATERIALS AND METHODS

Animals were maintained and handled in accordance with the guidelines issued by the Japan National Research Council and institutional guidelines at the RIKEN Brain Science Institute and the National Institute of Radiological Sciences. All experiments conducted here were approved by the Ethics Committees of the RIKEN Brain Science Institute and the National Institute of Radiological Sciences.

Generation of CS/APP double-transgenic (dTg) and CS-KO/APP-Tg mice

APP23 mice, which overexpress Swedish double-mutant APP751 under the control of a neuron-specific Thy-1 promoter element, were maintained as described previously on a C57BL/6J background (1). CS-KO mice were as described previously (17). The heterozygous CS-KO mice were crossbred with APP23 mice to obtain offspring heterozygous for both the CS-KO gene and the APP transgene; these animals were then mated with homozygous CS-KO mice to produce APP single-Tg mice homozygous for the CS-KO gene. CS/APP-dTg mice were developed by crossbreeding heterozygous CS-Tg mice with APP23 mice. Offspring were weaned from their mothers at the age of 4 wk, and tail samples were collected on this separation. The genotypes of the mice were determined by PCR with specific primer sets, as described previously (1, 17, 18). Mice dying before genotyping and injured from fighting were excluded from mortality assays.

Immunohistochemical and histochemical assays

Paraffin-embedded blocks of AD brains, fixed with 70% ethanol in isotonic saline, were kindly provided by John Q. Trojanowski (University of Pennsylvania School of Medicine, Philadelphia, PA, USA). Sections (5 μm thick) were generated from the tissue blocks and used for immunohistochemistry.

Mice were deeply anesthetized with pentobarbital, then transcardially perfused with 15 ml of phosphate-buffered saline followed by 15 ml of either 70% ethanol in isotonic saline or 4% paraformaldehyde in phosphate buffer (PB). Ethanol-fixed brains were embedded in paraffin, and representative 5-μm-thick sections were generated. Brain samples fixed with paraformaldehyde were serially immersed in PB containing 10 and 25% sucrose, and 10-μm-thick frozen sections were prepared.

Neurodegeneration was assessed by cresyl violet and hematoxylin-and-eosin staining. Immunofluorescence staining was performed using either a standard protocol (20) or the tyramide signal amplification (TSA) method using a TSA-Direct kit (NEN Life Science Products, Boston, MA, USA). For double and triple immunolabeling, we used a TSA-based technique. Amyloid staining with 1-fluoro-2,5-bis(3-carboxy-4-hydroxystyryl)benzene (FSB) was performed as in our previous studies (21). We also conducted Gallyas silver and thioflavin-S (Waldeck, Münster, Germany) staining as described elsewhere (4). In addition, apoptotic cell death was monitored by terminal deoxynucleotidyl transferase deoxyuridine triphosphate nick end labeling (TUNEL) with the aid of an *in situ* cell death detection kit (Roche Applied Science, Indianapolis, IN, USA).

Biochemical analysis of brain and cerebrospinal fluid (CSF) samples

Protein samples from mouse brains were prepared for immunoblotting, as described previously (18). Samples obtained from a WT C57BL/6J mouse intracranially injected with kainic acid (18, 20) were used as positive controls. John Q. Trojanowski (University of Pennsylvania School of Medicine) generously provided frozen brain tissues from autopsy-con-

firmed AD cases. Proteins were extracted from the tissues as described above.

We also analyzed calpain activation in living human subjects by assaying CSF samples from 14 patients (mean±SD age 73.7±6.3 yr) who were diagnosed as having AD according to the National Institute of Neurological and Communicative Disorders and Stroke–Alzheimer's Disease and Related Disorders Association (NINCDS-ADRDA) criteria and scored 17.0 ± 5.1 points (mean±SD) in the Mini-Mental State Examination. Nine age-matched normal subjects were used as controls (mean age 66.1±8.7 yr). The samples, which were kindly provided by Hiroyuki Arai (Tohoku University School of Medicine, Sendai, Japan), were stored at −80°C pending assay. To prepare baseline and positive controls, we collected CSF from 3 untreated and 3 kainate-injected mice using an established technique (22). The samples in each mouse group were combined into a pooled volume. All CSF preparations were first processed using a ProteoExtract Albumin/IgG Removal Kit (Calbiochem, San Diego, CA, USA) and thereafter with the SDS-PAGE Clean-Up Kit (GE Healthcare Japan, Tokyo, Japan). Aliquots (40 μl) of samples were used for SDS-PAGE.

Levels of APP and its proteolytic fragments were assessed by immunoblotting and ELISA as detailed elsewhere (23, 24). Mice were administered an overdose of pentobarbital, and brain tissues were dissected. The right neocortical samples were homogenized with 3 vol of homogenization buffer (50 mM Tris-HCl buffer, pH 7.6, containing 150 mM NaCl and protease inhibitor cocktail), and centrifuged at 200,000 *g* for 20 min at 4°C. The resultant pellet was rehomogenized with 3 vol of homogenization buffer plus 1% Triton X-100, and centrifuged at 200,000 *g* for 20 min at 4°C. The supernatant was then used as the membrane-associated fraction. Alternatively, a subportion of the pellet produced by the first centrifugation was resuspended in sample buffer. The 3 fractions (soluble, membrane-associated, and pellet) were then used for immunoblotting. Quantification of Aβ by sandwich ELISA was performed as described previously (3). In immunoblotting experiments, signals were developed using either the ECL Plus or ECL Advance kit (GE Healthcare Japan), detected with a LAS3000 densitometer (Fujifilm, Tokyo, Japan), and quantified using Image Gauge software (Fujifilm).

Tracing of commissural axons from hippocampal neurons

Recombinant adeno-associated viral vector expressing mutant, nonfunctioning human neprilysin (rAAV-NEP-MUT) was prepared as described previously (23). APP-Tg mice aged 18–19 mo were anesthetized with pentobarbital, after which 0.2 μl of rAAV-NEP-MUT solution (~0.36×10^{10} genome copies) was injected into the right hippocampal dentate gyrus using a 1-μl motorized Hamilton syringe (Hamilton, Reno, NV, USA; stereotactic coordinates: anteroposterior, 2.4 mm; mediolateral, 2.0 mm; and dorsoventral, 2.0 mm). Three months later, paraffin sections were generated as described above. As overexpressed neprilysin was primarily localized to the axonal and presynaptic compartments (23), the pattern of neprilysin immunostaining provided a map of the commissural projections from the injected region.

Autoradiographic quantification of glial activity

Glial activity in the brains of the mutant mice at 15 mo of age was quantified by autoradiographic analysis of paraformaldehyde-fixed, frozen brain sections using [^{3}H]DAA1106, a radioligand for translocator proteins, according to the method described for [^{11}C]DAA1106 (25). [^{3}H]DAA1106 was synthesized using its demethylated precursor (DAA1123; provided by Taisho Pharmaceutical, Tokyo, Japan), and purified by semipreparative HPLC (25). The brain sections were preincubated in 50 mM Tris-HCl buffer (pH 7.4) at room temperature for 15 min, and reacted with 0.5 nM [^{3}H]DAA1106 (radioactive concentration, 2.4 kBq/ml) in 50 mM Tris-HCl buffer (pH 7.4) at 25°C for 60 min. Nonspecific binding of the radioligand was determined by coincubation with 10 μM of PK11195 (Sigma-Aldrich, St. Louis, MO, USA). The samples were subsequently rinsed twice with ice-cold Tris-HCl buffer for 2 min and with ice-cold H_2O for 10 s (25). Radioactive signals were detected using a BAS-MS2025 imaging plate (Fujifilm) and a BAS5000 image analyzer (Fujifilm). Radiolabeling intensity corrected for nonspecific radioligand binding was measured using Multi Gauge software (Fujifilm).

Small-animal positron emission tomography (PET) imaging

PET scans of aged APP-Tg and CS-KO/APP-Tg mice were conducted as described elsewhere (26). Prior to PET analysis, anatomical template images were generated by scanning a C57BL/6J mouse head embedded in 3% aqueous agarose by a 9.4-T AVANCE 400WB imaging spectrometer (Bruker BioSpin, Ettlingen, Germany), as described previously (21). Coronal T2-weighted magnetic resonance (MR) images were acquired using a 3-dimensional (3D) fast-spin echo sequence. PET scans were then performed with a microPET Focus 220 animal scanner (Siemens Medical Solutions, Knoxville, TN, USA), which provides 95 transaxial slices 0.815 mm apart. Animals were anesthetized with 1.5% (v/v) isoflurane, and emission scans were acquired for 60 min in a 3D list mode, immediately after intravenous injection of [^{11}C]Pittsburgh compound B (PIB; 31.9±7.2 MBq) radiosynthesized, as documented previously (26). All list-mode data were sorted into 3D sonograms, which were then Fourier rebinned into 2-dimensional sonograms. Dynamic images were reconstructed with filtered backprojection using a 0.5-mm Hanning's filter. Volumes of interest were placed on the hippocampus and cerebellum using PMOD image analysis software (PMOD Group, Zurich, Switzerland) with reference to the MR imaging template. Amyloid load in living mice was quantified by estimating nondisplaceable binding potential (BP_{ND}) for [^{11}C]PIB with the use of the simplified reference tissue model (26).

Antibodies

The following antibodies were used for monitoring the calpain-CS system and caspases: rabbit polyclonal antibodies against the calpain-cleaved carboxyl-terminal 150-kDa fragment of α-spectrin (150kf; 1:200 dilution; refs. 27, 28) and amino-terminal 136-kDa fragment of α-spectrin (136kf; 1:2000; refs. 17, 18); mouse monoclonal antibody against the carboxyl-terminal of α-spectrin (AA6; 1:1000; Biohit, Neptune, NJ, USA); rabbit polyclonal antibody against the caspase-cleaved amino-terminal 32-kDa fragment of actin (fractin; Clact32; 1:2000; refs. 17, 18); rabbit polyclonal antibodies against mouse CS (1:1000), mouse m-calpain (1:5000; ref. 28), μ-calpain (1:1000; ref. 29) and calpain-10 (1:1000; Gene Tex, Irvine, CA, USA); goat polyclonal antibodies against caspase-3 (K-19; 1:1000; Santa Cruz Biotechnology, Santa Cruz, CA, USA) and caspase-6 (A-18; 1:1000; Santa Cruz Biotechnology); and rabbit polyclonal antibody against caspase-9 (H-83; 1:1000; Santa Cruz Biotechnology).

Cytoskeletal constituents other than α-spectrin and actin were analyzed with the following antibodies: mouse monoclonal antibodies against nonphosphorylated neurofilament

high-molecular-weight subunit (NFH; RMdO9; 1:500), phosphorylated NFH (RMO24; 1:500), and phosphorylated/non-phosphorylated neurofilament middle molecular weight subunit (RMO189; 1:500) (4); rabbit antiserum against the neurofilament low-molecular-weight subunit (αNFL; 1:1000) (4); and mouse monoclonal antibodies against phosphorylated tau (AT8; 1:2000; Innogenetics, Gent, Belgium), MAP2 (AP20; 1:10; Roche Applied Science), and α-tubulin (DM1A; 1:1000; Sigma-Aldrich).

We also assessed synaptic components using rabbit polyclonal antibodies against synaptic vesicle glycoprotein 2A (SV2A; 1:100; Calbiochem-Novabiochem, San Diego, CA, USA), synaptosomal-associated protein 25 (SNAP-25; 1:200; Santa Cruz Biotechnology), glutamate receptor type 1 (AB1504; 1:1000; Millipore-Chemicon, Temecula, CA, USA), metabotropic glutamate receptor type 2/3 (1:1000; Millipore-Chemicon) and growth-associated protein 43 (GAP43; AB5220; 1:2000; Millipore-Chemicon), mouse monoclonal antibody against postsynaptic density-95 protein (PSD-95; clone 7E3–1B8; 1:1000; Millipore-Chemicon), and goat polyclonal antibody against the $GABA_A$ receptor α1 subunit (1:5000; Santa Cruz Biotechnology).

The metabolism of APP and Aβ was investigated using the following antibodies: mouse monoclonal antibodies against the N-terminal of APP (22C11; 1:5000; Millipore-Chemicon), a rabbit polyclonal antibody against the C-terminal of APP (A8717, 1 μg/ml; Sigma), APPs and Aβ (6E10; 1:1000; Signet Laboratories, Dedham, MA, USA), Aβ (4G8; 1:400), rabbit polyclonal antibodies against the amino-terminal portion of Aβ (N1D; 1:1,000) (30), and the carboxyl-terminal portion of Swedish mutant APPsβ (βNL; 1:1000; ref. 24). Neprilysin was assessed biochemically and histochemically using goat polyclonal antibody (AF1126; 1 μg/ml; R&D Systems, Minneapolis, MN, USA) and mouse monoclonal antibody (56C6; 1:200; Novocastra, Newcastle, UK).

RESULTS

Calpain and caspase activation in brains of patients with AD and of APP-Tg mice

Application of our polyclonal antibodies raised against 136kf (also known as fodrin; ref. 17) revealed prominent activation of calpain in the hippocampus and neocortex of postmortem AD brains (**Fig. 1**). The 136kf antibody differs from an alternative antibody against 150kf (28) in that it can be applied to a paraffin-embedded section, making it the antibody of choice for the ethanol-fixed paraffin-embedded human tissues used in the present study. Intense 136kf immunolabeling was primarily observed as an annular cluster surrounding an Aβ-positive senile plaque (Fig. 1*A–C*). Triple immunofluorescence staining with antibodies recognizing 136kf, phosphorylated tau, and Aβ also allowed us to observe a correlation between calpain activation and intraneuronal/extraneuronal amyloid lesions at different stages of plaque formation (Fig. 1*D–S*). Circular deposition of 136kf emerged in an area showing faint tau and Aβ immunoreactivities (Fig. 1*D–G*). The 136kf signals were also specifically noted in compact (Fig. 1*H–K*) and dense-core neuritic (Fig.

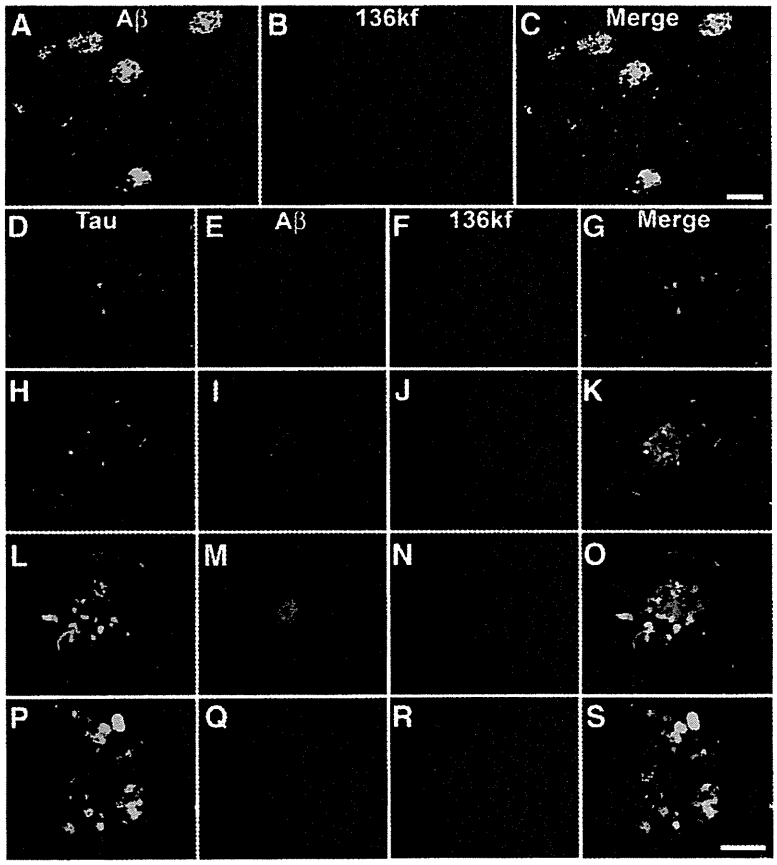

Figure 1. Calpain activation occurred in close apposition to senile plaques in the brain of patients with AD. *A–C*) Paraffin section of the frontal cortex from a patient with AD was doubly immunolabeled with antibodies against Aβ (4G8; *A*) and 136kf (*B*); 2-channel confocal fluorescence micrograph (*C*) illustrates that calpain-mediated proteolysis of α-spectrin took place primarily in the vicinity of amyloid plaques. *D–S*) Accumulation of calpain cleavage products at different stages of plaque formation, captured in the temporal cortex by triple immunofluorescence staining (triple-channel; *G, K, O, S*) for phosphorylated tau (AT8; *D, H, L, P*), Aβ (N1D; *E, I, M, Q*), and 136kf (*F, J, N, R*). Activation of calpain was captured in a diffuse plaque (*D–G*), and was more prominent in compact (*H–K*) and dense-core (*L–O*) plaques. Proteolyzed α-spectrin was less abundant in mature neuritic plaques (*P–S*), with faint staining present mostly in tau-immunoreactive dystrophic neurites. Scale bars = 100 μm (*A–C*); 50 μm (*D–S*).

1*L–O*) plaques, whereas minimal overlap was found between 136kf immunolabeling and phosphorylated tau-immunoreactive dystrophic neurites (Fig. 1*L–O*).

Accumulation of calpain-cleaved α-spectrin in plaques showing abundant mature neuritic tau aggregates was found at a much lower level than that observed in other types of plaques, and there was only partial colocalization with phosphorylated tau staining (Fig. 1*P–S*). Calpain activation was not apparent in the vicinity of diffuse plaques with weak Aβ labeling (data not shown). Although the diversity of plaque morphology does not necessarily reflect the temporal sequence of plaque formation, these observations suggest that an increase in calpain activity occurs relatively early in the generation of the pathological plaques characteristic of AD.

To compare the pattern of calpain and caspase activation, we performed triple immunolabeling of AD brain sections using an antibody against Clact32 (17). Similar to calpain, caspase was activated in the close proximity to compact and dense-core plaques, although the 136kf and Clact32 signals did not colocalize (**Fig. 2*A–D***). Because α-spectrin and actin are ubiquitously present in neurons and glia, this result can be attributed to activation of calpain and caspase at distinct cellular compartments associated with plaques.

We also applied the triple-labeling technique to frozen brain sections obtained from a widely used APP-Tg mouse strain known as APP23 (1). Frozen brain sections, which could only be generated from experimental animals, were used to assess calpain activation. Here, we used the antibody against 150kf (28), as this antibody is more sensitive and specific than 136kf on frozen sections and because a number of the other antibodies used for double and triple staining are applicable only to frozen sections. Investigation of 24-mo-old Tg mice revealed that accumulation of the products of calpain- and caspase-catalyzed proteolysis occurred at high levels in the vicinity of Aβ (Fig. 2*E–H*), demonstrating the parallels between enzymatic cytoskeletal disruption in this mouse model and human AD pathology. In addition, it is noteworthy that the activity of the two proteases was mostly nonoverlapping (Fig. 2*H*). Clact32 and 150kf immunoreactivity was also found to surround smaller amyloid plaques in 12- and 15-mo-old APP-Tg mice and was barely distinguishable from nonspecific signals in younger mice bearing no visible Aβ deposits (data not shown). Cerebrovascular Aβ deposits were not associated with 136kf, 150kf, and Clact32 immunolabeling in APP-Tg mice even at 26 mo of age (data not shown). In line with accumulation of fragmented α-spectrin and actin, m-calpain and caspase-3 were localized in the periphery of Aβ plaques (Fig. 2*I–L*). These data indicate that the calpain and caspase activation observed in AD brains is not a postmortem artifact. We could not detect the presence of μ-calpain or other caspases, presumably due to the limited sensitivity of the antibodies employed.

In accordance with these neuropathological results, our biochemical data also supported the notion that AD pathology accelerates calpain-catalyzed cytoskeletal

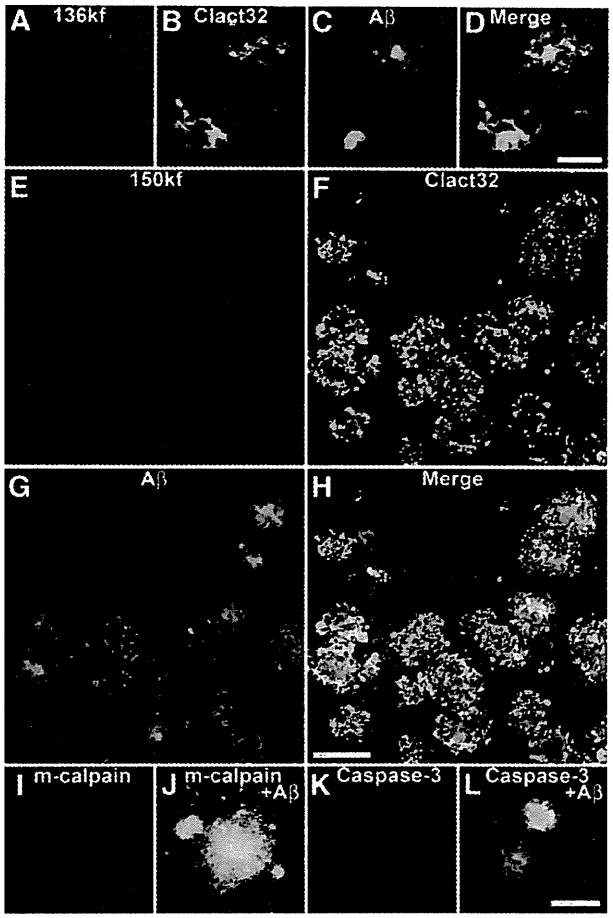

Figure 2. Enhancement of calpain and caspase activity in distinct plaque-surrounding compartments in the brains of patients with AD and APP-Tg mice. *A–D*) Calpain-cleaved α-spectrin (136kf; *A*) and caspase-cleaved actin (Clact32; *B*) accumulate at sites contacting Aβ plaques (4G8; *C*) in the temporal cortex of a patient with AD patient; confocal triple fluorescence illustrates little overlap between 136kf and Clact32 signals (*D*). *E–H*) In 24-mo-old APP-Tg mice, fine granuloreticular immunolabeling of calpain-proteolyzed α-spectrin (150kf; *E*) accompanied globular Clact32 immunoreactivity (*F*) in the vicinity of amyloid plaques (4G8; *G*), as detected by triple-fluorescence labeling; colocalization of calpain and caspase activation was confined to a very small subset of immunolabeled areas (*H*). *I–L*) Concentration of m-calpain (*I, J*) and caspase-3 (*K, L*) in the periphery of 4G8-immunostained Aβ plaques in a 24-mo-old APP-Tg mouse. Scale bars = 50 μm (*A–D, I–L*); 100 μm (*E–H*).

degradation (**Fig. 3**). Levels of 136kf increased significantly in the hippocampi of APP-Tg mice as compared to WT controls (Fig. 3*A, B*). The same immunoblotting protocol also detected enhanced production of 136kf in neocortical samples from patients with AD (Fig. 3*A*). However, the cerebellum, which is known to develop only limited AD pathology, likewise exhibited modest 136kf deposition (Fig. 3*A*), implying a substantial effect of postmortem proteolysis, as previously reported (31). To address this issue, therefore, we also examined the levels of intact and fragmented α-spectrin in CSF collected from living patients with AD, thereby mini-

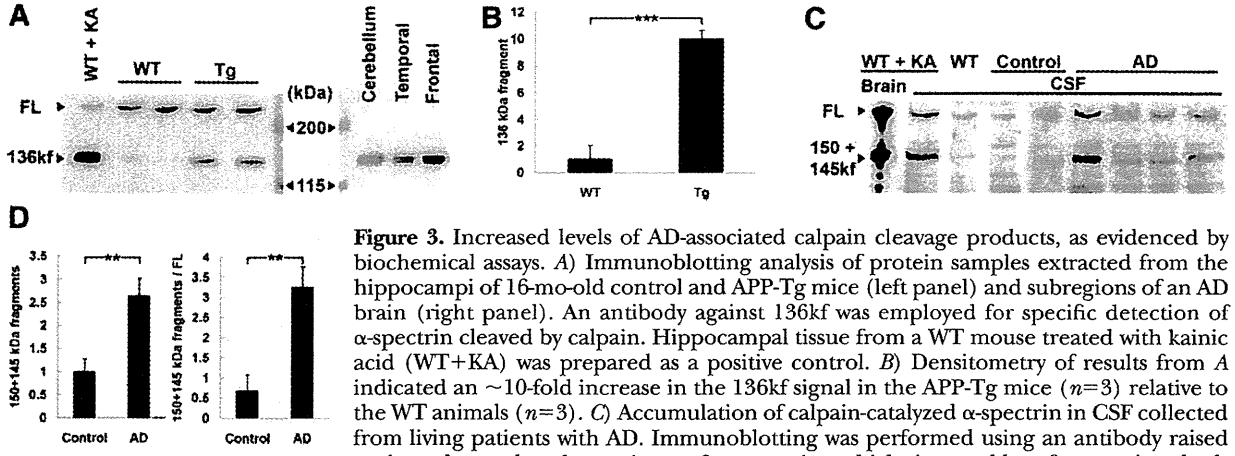

Figure 3. Increased levels of AD-associated calpain cleavage products, as evidenced by biochemical assays. *A*) Immunoblotting analysis of protein samples extracted from the hippocampi of 16-mo-old control and APP-Tg mice (left panel) and subregions of an AD brain (right panel). An antibody against 136kf was employed for specific detection of α-spectrin cleaved by calpain. Hippocampal tissue from a WT mouse treated with kainic acid (WT+KA) was prepared as a positive control. *B*) Densitometry of results from *A* indicated an ~10-fold increase in the 136kf signal in the APP-Tg mice (n=3) relative to the WT animals (n=3). *C*) Accumulation of calpain-catalyzed α-spectrin in CSF collected from living patients with AD. Immunoblotting was performed using an antibody raised against the carboxyl terminus of α-spectrin, which is capable of capturing both full-length and fragmented proteins. Brain tissue and CSF samples pooled from 3 kainate-treated mice (WT+KA), together with those from 3 untreated mice (WT), were used as positive and baseline controls, respectively. Similar to WT + KA samples, increased immunoblotting signals corresponding to full-length α-spectrin (FL) and the conjunction of 150- and 145-kDa fragments cleaved by calpain (150+145 kf) were observed in the CSF from patients with AD, as compared with age-matched controls. *D*) Quantification of the signal intensity in *C* demonstrated an elevated level of calpain-cleaved fragments (left panel), as well as an increase in the ratio of cleaved to full-length species (right panel) in AD CSF (n=14) as compared with control CSF (n=9). $^{**}P < 0.01$, $^{***}P < 0.001$ (t test).

mizing nonessential protein degradation (Fig. 3*C, D*). As full-length α-spectrin was increased in AD CSF relative to CSF from control subjects, it is conceivable that cytoskeletal components emanated from injured neurons in a similar manner to tau. More importantly, the levels of calpain-generated 150- and 145-kDa fragments of α-spectrin exceeded the amount of full-length protein in AD CSF, and the ratio of the breakdown products to the intact protein in the CSF of patients with AD was significantly increased as compared to that of control subjects. These observations clearly demonstrate calpain hyperactivation in the brains of living patients with AD.

Aberrant neurite growth and synaptic terminal formation linked to amyloidosis and protease activation

We further aimed to identify subcellular compartments in which calpain and caspase proteolyze cytoskeletal proteins in APP-Tg mice. Neither 150kf nor Clact32 colocalized with neurofilament subunits, tau, or MAP2 (data not shown), thus excluding the possibility that neuritic processes are primary sites of calpain- and caspase-mediated cytoskeletal disruptions. In contrast, a significant subset of synaptic markers encircled Aβ plaques in association with either 150kf or Clact32 (**Fig. 4**). Caspase activation colocalized with the presynaptically localized protein SV2A (Fig. 4*A–D*): calpain activation overlapped with $GABA_A$ receptor subunit 1α expressed at postsynaptic termini (Fig. 4*E–H*). Caspase activation was also detected in enlarged synaptic boutons contacting amyloid plaques and was associated with up-regulation of GAP43 (Fig. 4*I, J*). All these synaptic components, together with 136kf and Clact32 signals, also surrounded Aβ plaques located in the subcortical white matter, which is typically asynaptic (data not shown). Immunolabeling for PSD-95 was diminished in the proximity of plaques, consistent with previous observations (32), and was spatially overlapped with intensification of 150kf immunolabeling (Fig. 4*K, L*), implying loss of excitatory postsynaptic components in concurrence with calpain activation.

The involvement of calpain in the pathological formation of synaptic termini and neurite extension was further evidenced by axonal tract tracing in APP-Tg mice (Fig. 4*M–P*). Unilateral administration of adeno-associated virus carrying inactive human neprilysin cDNA into the hippocampal dentate gyrus led to expression of the protein in ipsilateral neurons at a level exceeding that of endogenous neprilysin (23); this enabled us to track the projection of commissural fibers to the contralateral hippocampus. We observed neurite sprouting toward an amyloid aggregate in the middle molecular layer, whereas these axons normally terminate at the inner molecular layer of the dentate gyrus. Moreover, termini of the aberrantly extended neurites were apposed to sites of calpain activation. In this consideration, there is a possibility that calpain was activated at outgrowing neuritic terminals, as well as dendritic spines in association with $GABA_A$ receptors as indicated in a previous report (33). Hereafter, we focused only on the role of calpain because caspase inhibition does not protect neurons from excitotoxicity (18, 20) and because there was no detectable DNA fragmentation in any of the mouse strains used here.

Mortality and neurodegeneration in CS-deficient APP-Tg mice

To modulate the calpain-CS system in APP-Tg mice, we crossbred APP23 mice with CS-Tg and CS-KO mice.

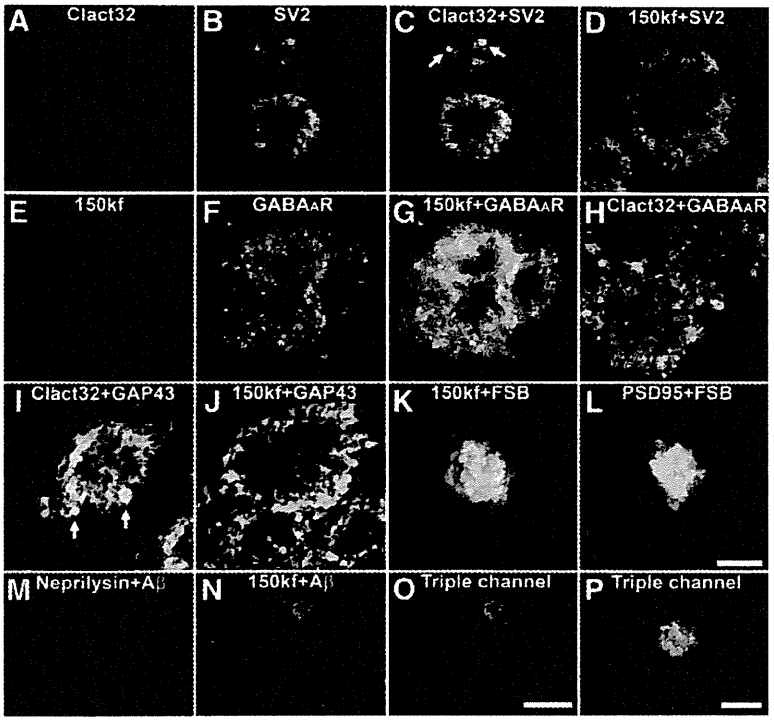

Figure 4. Involvement of calpain and caspase in aberrant axonal growth associated with amyloid plaques in the APP-Tg mouse brain. *A–D*) Double-immunofluorescence staining of amyloid plaques, showing localization of Clact32 signals (*A*) closely associated with the presynaptic marker SV2 (*B*, and double channel in *C*), whereas 150kf immunoreactivity (*D*, red) poorly colocalized with SV2 labeling (*D*, green). Enlarged synaptic termini (*C*, arrows) contained colocalized Clact32 and SV2 signals. *E–H*) In the case of 150kf (*E*) and $GABA_AR1\alpha$ (*F*) immunoreactivity, there was fine colocalization (double channel in *G*); in contrast, little colocalization of Clact32 (*H*, red) and $GABA_AR1\alpha$ (*H*, green) immunoreactivity was observed in the vicinity of plaque lesions. *I, J*) Clact32 immunolabeling appeared consistent with the distribution of GAP43 (*I*), which only partially colocalized with 150kf (*J*) in areas surrounding plaques. Swollen synaptic boutons (*I*, arrows) were immunoreactive for both Clact32 and GAP32. *K, L*) Immunostaining for 150kf (*K*, red) and PSD-95 (*L*, red) in the periphery of plaques detected by FSB (blue) in subadjacent neocortical sections, illustrating a tight link between calpain activation and loss of excitatory postsynaptic elements. *M, N*) Axonal termini of fibers growing aberrantly toward Aβ plaques. Commissural fibers, traced using the axonal/presynaptic marker neprilysin (*M*, red) overexpressed in the contralateral hippocampus, normally terminate in the inner molecular layer of the dentate gyrus. However, in pathological cases, these fibers extended to the proximity of Aβ-positive plaques (*M, N*, blue) expressing 150kf (*N*, green) located in the middle molecular layer. *O, P*) Colocalization of the 150kf signal with the endings of ectopic nerves is explicitly illustrated in triple-channel photomicrographs at low magnification (*O*) and high magnification (*P*). Scale bars = 50 μm (*A–L, P*); 100 μm (*M–O*).

CS-Tg mice display ~3 times greater calpain-inhibiting activity than wild-type (WT) controls (17). In contrast to the insignificant changes in the survival of CS-KO mice compared with WT animals, APP-Tg mice died an average of 12 wk earlier (Supplemental Fig. S1). CS deficiency significantly decreased the survival time of APP-Tg mice in a gene dose-dependent manner: 50% of APP-Tg mice homozygous for the CS-KO allele died by 15 wk of age, long before the emergence of amyloid lesions in the brain, whereas half of the APP-Tg mice survived for >50 wk. Because calmodulin kinase II promoter-driven CS overexpression resulted in significantly longer survival of APP-Tg mice (Supplemental Fig. S1), neuronal CS alone seems to influence the outcome for these animals. Despite their short life span, no overt motor or behavioral phenotypes were noted in the CS-KO/APP-Tg mice. However, because of the sudden unexpected death of these mutant mice, we were unable to perform behavioral tests.

Neuropathological examination revealed remarkable degenerative changes in the CS-KO/APP-Tg mice at 6 mo of age (**Fig. 5**). Pyramidal neurons displaying apparent atrophy of the soma (Fig. 5*A–C*) and severe apical dendrite dystrophy (Fig. 5*D–F*) were observed exclusively in a subpopulation (~1/3) of the CS-KO/APP-Tg mice. Immunohistochemistry using anti-phosphorylated tau antibody (AT8) also highlighted punctate lesions in the hippocampal subiculum of the APP-Tg mice. Tau phosphorylation, hardly detectable in nontransgenic mice, was significantly enhanced by CS deficiency and diminished by CS overexpression (Fig. 5*G–L*). This immunoreactivity did not colocalize with the expression of neurofilament subunits, MAP2, or α-tubulin (data not shown), suggesting that the phosphorylated tau revealed here was probably cytoplasmic rather than being found in the regular cytoskeletal architecture. These lesions were negative for silver impregnation, FSB, and thioflavin-S, unlike neurofibrillary tangles in AD brains. No increase in the 150kf, 136kf, or Clact32 signal was observed in any of the mouse strains at 6 mo of age. Hence, the pathological changes that we have identified in the CS-KO/APP-Tg mice are likely to have arisen from undetectably low-level, but chronic, activation of calpain, which only becomes evident at later ages (see Fig. 3 and the following sections). Despite evidence for neurodegenerative pathologies in CS-KO/APP-Tg mice, we never detected TUNEL signals in any of the mice (3–16 mo old) investigated in this study (data not shown). Our positive controls were mouse brains treated with kainate (17).

Effect of altered CS levels on Aβ amyloidosis

We next analyzed the neuropathology of 15-mo-old mutant mice, this being the age at which the animals displayed detectable Aβ deposition (**Fig. 6**). As only a limited number of CS-KO/APP-Tg mice survived this

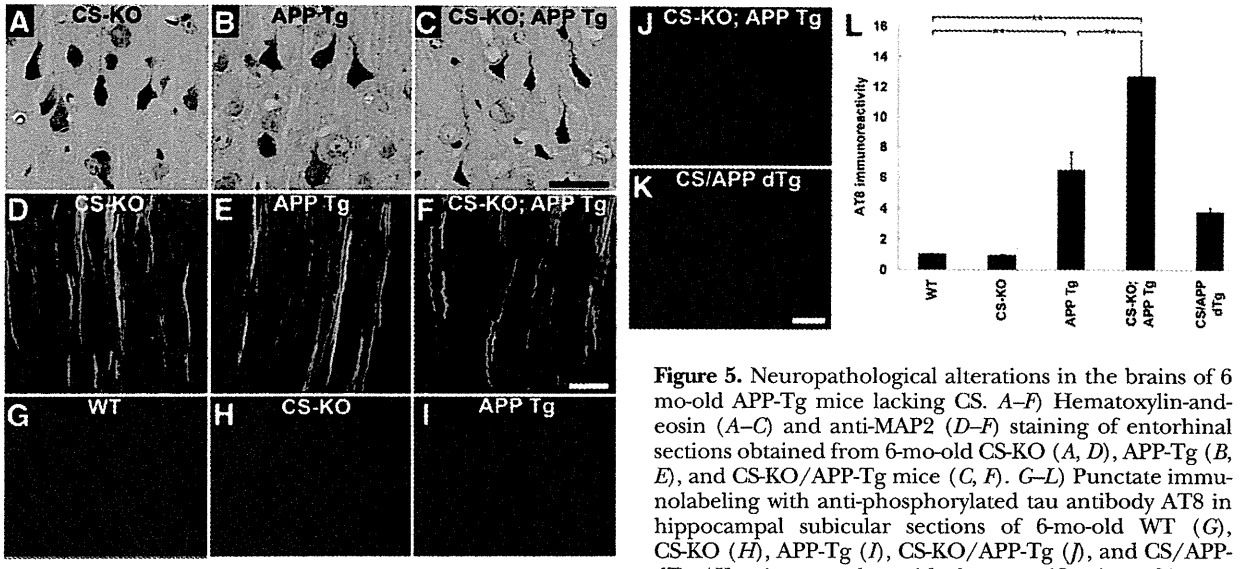

Figure 5. Neuropathological alterations in the brains of 6 mo-old APP-Tg mice lacking CS. *A–F*) Hematoxylin-and-eosin (*A–C*) and anti-MAP2 (*D–F*) staining of entorhinal sections obtained from 6-mo-old CS-KO (*A, D*), APP-Tg (*B, E*), and CS-KO/APP-Tg mice (*C, F*). *G–L*) Punctate immunolabeling with anti-phosphorylated tau antibody AT8 in hippocampal subicular sections of 6-mo-old WT (*G*), CS-KO (*H*), APP-Tg (*I*), CS-KO/APP-Tg (*J*), and CS/APP-dTg (*K*) mice, together with the quantification of immunofluorescence intensity (*L*). Clustered punctate immunolabeling was observed exclusively in mice overexpressing APP (*I–K*) and was markedly enhanced by the lack of CS (*J*), the interstrain differences being indicated by statistical analysis of the intensitometric data (*L*). Despite scattered signals found in CS/APP-Tg mice (*K*), quantified immunoreactivity did not significantly differ from that of APP-Tg and WT mice (*L*). This indirectly indicates attenuation of tau phosphorylation in APP-Tg mice, as these animals showed significant elevation of AT8 immunoreactivity. $*P < 0.05$ (Fisher's least-square difference *post hoc* test following 1-way ANOVA). Error bars = SE. Scale bars = 50 μm (*A–F*); 100 μm (*G–K*).

long (Supplemental Fig. S1), we used 5 males in each group of control and mutant animals. In contrast to CS overexpression, which diminished Aβ deposition, CS deficiency led to a substantial (~10-fold) increase in Aβ load, as demonstrated by staining with 4G8 (Fig. 6*A–D*) and a fluorescent amyloidophilic dye, FSB (ref. 21 and data not shown; $P<0.05$ by t test). The onset of Aβ deposition in CS/APP-dTg mice (at ~10 mo of age) was slightly retarded relative to that in APP-Tg mice (at ~8 mo), but this difference was not statistically significant (data not shown). In addition, plaques developed in CS/APP-dTg and CS-KO/APP-Tg mice were morphologically similar to those in APP-Tg mice. The change in amyloid load in the CS/APP-dTg and CS-KO/APP-Tg mice was accompanied by remarkable attenuation and elevation of 150kf immunoreactivity, respectively (Fig. 6*E–G*). As there was a significant primary effect of genotype on the ratio of 150kf immunoreactivity to amyloid burden (Fig. 6*H*), suppression of calpain activation in the dTg mice did not seem to be merely secondary to decreased Aβ accumulation. There was also extensive accumulation of calpain-mediated breakdown products in the CS-KO/APP-Tg mice (Fig. 6*E, G*), with 150kf/4G8 ratios in the two genotypes, suggesting that the increment of calpain activity exceeded the enhancement of Aβ pathology (Fig. 6*H*). By contrast, the ratio of Clact32 immunoreactivity to 4G8-positive plaque load did not significantly differ among the APP-Tg, CS-KO/APP-Tg and CS/APP-dTg mice (data not shown). In addition, microglial activation was up-regulated in the CS-KO/APP-Tg mice and down-regulated in the CS/APP-dTg animals as compared to littermate controls (Fig. 6*I–L*). Deposition of Aβ was also longitudinally investigated in the same individuals from 18 to 26 mo of age with the aid of small-animal PET and an amyloid-binding radioligand, [^{11}C]PIB. At 18 and 22 mo of age, enhanced neocortical and hippocampal accumulation of Aβ was observed in the CS-KO/APP-Tg mice relative to the APP-Tg animals (Fig. 6*M–P*), although the difference between these two genotypes became less significant with aging (Fig. 6*Q*). The significant contribution of CS to the regulation of Aβ-related pathology was further evidenced by CS immunoreactivity encircling the amyloid plaques of APP-Tg mice (Fig. 6*R–T*), an effect that disappeared in CS-KO/APP-Tg animals (Fig. 6*U–W*). Our preliminary assays also indicated that this plaque-associated CS immunoreactivity in APP-Tg mouse brains increased from 18 to 26 mo of age by ~60%, which was much smaller than the increase of 150kf immunolabeling (~170%) during the same period (data not shown). This finding may provide an explanation for the age-dependent diminution of the effect of CS deficiency as assessed by PET, and implies that CS exerted a major regulatory role in Aβ amyloidogenesis at a relatively early stage. AT8 immunoreactivity in plaque-associated dystrophic neurites was intensified in CS-KO/APP-Tg mouse brains relative to APP-Tg mice, but they were not detectable by silver, FSB and thioflavin-S staining (data not shown).

To circumvent alterations secondary to plaque formation, biochemical assays of APP/Aβ and related molecules were also performed on young (2-mo-old) mice (Supplemental Fig. S2). None of these proteins and peptides, except the γ-secretase-cleaved C-terminal fragment of APP (AICD; Supplemental Fig. S2*D*), was noticeably different in the neocortex of CS-KO/APP-Tg mice, as compared with APP-Tg animals. The level of

neprilysin tended to be lower in the CS-KO/APP-Tg mice, but the difference between the two genotypes did not reach statistical significance (Supplemental Fig. S2*E*). Unlike this immunoblotting result, fluorometric measurements demonstrated a reduction in neprilysin activity in CS-KO/APP-Tg mice (**Fig. 7*A***). Since no marked alterations in this enzymatic activity were observed in single CS-KO and APP-Tg mice, there may be a synergistic impact of calpain activation and APP/Aβ accumulation on neprilysin. Consistent with these data, immunohistochemical assessments showed significantly decreased levels of neprilysin in specific hippocampal regions, including the pyramidal layer in CA1 and CA2 and the terminals of mossy fibers (Fig. 7*B–D*), indicating reduced neprilysin localization to presynaptic compartments.

Finally, we investigated the involvements of distinct calpain subtypes in Aβ pathogenesis, revealing notable accumulation of calpain-10 in APP-Tg mouse brains. In contrast to the putative postsynaptic localization of 136kf and 150kf, the pattern of calpain-10 immunolabeling overlapped with that of a presynaptic marker protein, SNAP-25, in the vicinity of Aβ plaques (**Fig. 8*A–D***). In AD brains, intensified calpain-10 immunoreactivity was observed in dystrophic neurites surrounding plaques (Fig. 8*E*, *F*), which were also encompassed by enhanced SNAP-25 signals (Fig. 8*G*, *H*). Calpain-10 also colocalized with fibrillary tau lesions in these tissues, as exemplified by neurofibrillary tangles and neuropil threads (Fig. 8*I*, *J*) and could, therefore, mechanistically link Aβ and tau pathologies in the molecular and cellular etiology of AD.

DISCUSSION

One of the most striking effects of CS deficiency on APP-Tg mice observed in the present study was an increase in mortality. Although the underlying mechanisms are unclear, hyperactivation of neuronal calpain is likely to be primarily involved for the following reasons: transgene-derived APP is expressed exclusively in the brain (1); brain-specific CS overexpression lengthened the life span of APP-Tg mice; CS-KO/APP-Tg mice died suddenly in the absence of any prior symptoms; and no systemic abnormalities were noted in the mice after death.

The work presented here provides clear evidence of a bidirectional link between Aβ amyloidosis and the calpain-CS system in the brain. Although calpain activation has also been implicated in neurodegenerative processes in diverse non-AD neurological disorders, including Parkinson's and Huntington's diseases (34), promotion of amyloid formation by calpain, as demonstrated in this study, seems characteristic of the AD pathogenesis. The reciprocal enhancement of Aβ deposition and calpain up-regulation are likely to involve multiple molecular events, including cytoskeletal disorganization, loss of synaptic and neuritic integrity, and accumulation of abnormally phosphorylated tau proteins, driving neurons toward degenerative pathologies.

Of particular interest is the finding that the calpain-CS system influences pathological Aβ deposition. We would like to emphasize that the data obtained using brain and CSF samples from mutant mice and patients with AD produced consistent results. Although it is conceivable that APP fragments other than Aβ, such as APPs and the APP intracellular domain (3), may have interacted with the calpain-CS system in the APP-Tg mice, this possibility is unlikely, given that selective elevation of synapse-associated Aβ oligomers, without overproduction of the other APP fragments, alone caused synaptotoxicity and cognitive dysfunction (24).

How does pathogenic Aβ activate neuronal calpain? Soluble Aβ has been shown to induce degradation of PSD-95, and this cleavage requires *N*-methyl-D-aspartate (NMDA) receptor activity (35). Because PSD-95 is a substrate for calpain (36), calpain conceivably mediates postsynaptic impairments subsequent to NMDA receptor-dependent calcium influx. The NMDA-dependent calpain-catalyzed proteolysis of metabolic glutamate receptor 1α has also been reported (37). Furthermore, Aβ oligomers have been shown to cause MAP2 degradation in cortical neurons in a calpain-dependent manner (38). Hence, we believe that the dystrophic pathology of dendrites observed in CS-KO/APP-Tg mice is attributable to enhanced proteolytic activity of calpain in response to synaptotoxic Aβ oligomers (24) antecedent to the deposition of fibrillar Aβ. Aβ oligomers have also been shown to induce NMDA receptor-mediated calpain activation at synaptic termini in cultured hippocampal neurons, resulting in proteolytic degradation of dynamin 1, which is essential for the maintenance of synaptic integrity (39).

Furthermore, recent *in vivo* evidence that calcium overload in neurites, with subsequent increased neuronal activity, depends on the existence of APP-Tg amyloid plaques and occurs in proximity to these plaques has reinforced the idea that calpain is activated by fibrillar Aβ deposition. Such a calcium overload would disrupt spino-dendritic calcium compartmentalization and, in turn, cause distorted morphological changes in neuronal processes (11, 12). In fact, it has been reported that calpain activation occurs in the dendritic spines of cultured neurons treated with glutamatergic agonists (40). Thus, amyloid plaques impair neuritic calcium homeostasis, and consequently may cause calpain-mediated structural and functional disruption of neuronal networks in the AD brain.

Our finding that crossbred mutant mice exhibit altered levels of Aβ deposition offers better understanding of the mechanistic basis on which the calpain-CS system and Aβ metabolism are bidirectionally regulated. Recent investigation has shown that calpain inhibition increases α- and β-cleavage in cultured fibroblast-like cells, presumably due to altered subcellular localization of APP (41). The promotion of β-secretase expression by activated calpains has also been indicated in a recent experiment using CS-Tg mice crossbred with APP/presenilin-1-dTg mice (42). Our data, however, demonstrate that neither α- nor β-secretase activ-

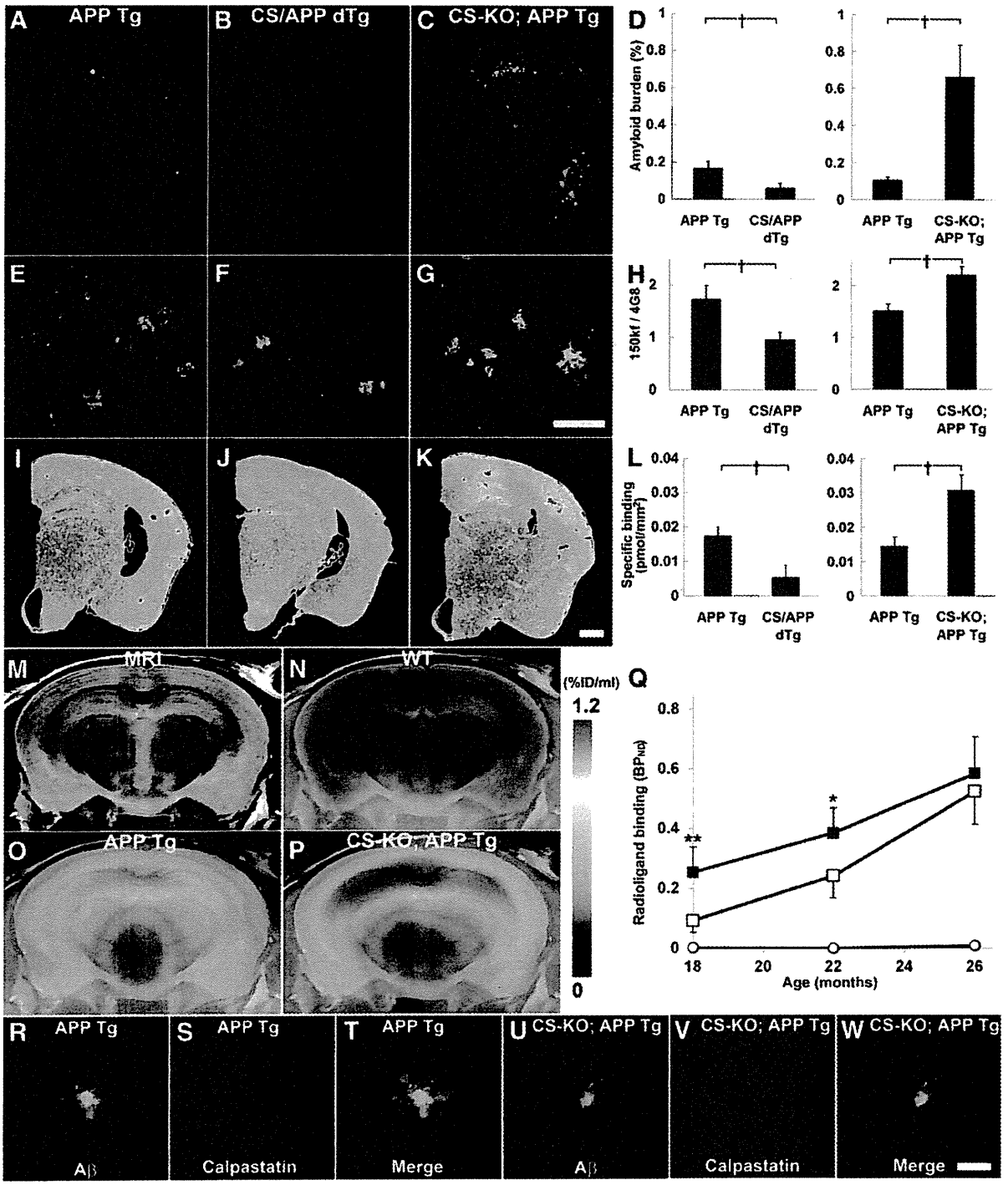

Figure 6. Amyloid-related pathologies are critically modified by the level of CS in APP-Tg mice. *A–C*) Immunofluorescence staining with 4G8 in 15-mo-old male APP-Tg (*A*), CS/APP-dTg (*B*), and CS-KO/APP-Tg (*C*) mouse brains. *D*) Comparison of amyloid load (percentage of measured area) between CS/APP-dTg and littermate APP-Tg mice (left panel; 3 males and 3 females/group) and between CS-KO/APP-Tg and littermate APP-Tg mice (right panel; 5 males/group). *E–G*) Double immunolabeling with 4G8 (green) and 150kf (red) for male APP-Tg (*E*), CS/APP-dTg (*F*), and CS-KO/APP-Tg (*G*) mouse brains. *H*) Quantified ratio of 150kf immunoreactivity to 4G8 signal. Comparison is done as in *D*. *I–K*) Autoradiographic images of activated glia in male APP-Tg (*I*), CS/APP-dTg (*J*), and CS-KO/APP-Tg (*K*) mouse brains. *L*) Specific radiotracer binding in the neocortical and hippocampal areas of the mice. Sample size and gender composition are as in *D*. *M–P*) *In vivo* amyloid PET imaging in 22-mo-old WT (*N*), APP-Tg (*O*), and CS-KO/APP-Tg (*P*) mice. Coronal PET images, taken 3 mm posterior to bregma, contain the neocortex and anterior hippocampus. These images were generated by averaging dynamic scan data at 30–60 min after intravenous injection of [^{11}C]PIB and were then overlaid on the MR imaging template (*M*). PET data are scaled

(*continued on next page*)

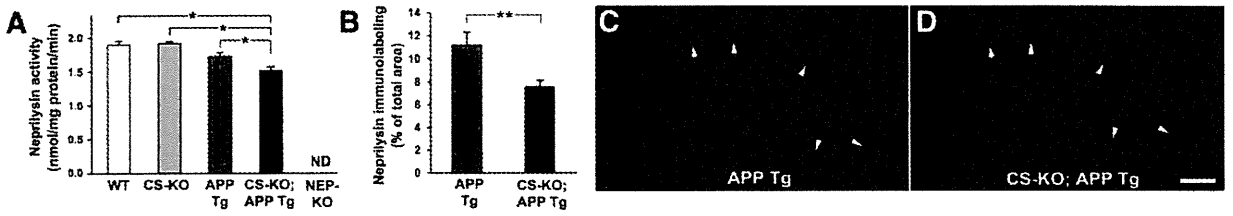

Figure 7. Early changes in the Aβ-degrading endopeptidase, neprilysin, as a consequence of crosstalk between the APP/Aβ and calpain-CS systems. *A*) Fluorometrically assayed neprilysin activity in the neocortex of 2-mo-old mice (n=6–9). ND, not detectable. Two-way ANOVA showed a significant primary effect of the APP transgene [$F_{(1,35)}$=28.046, P<0.0001] but no such effect of CS deficiency [$F_{(1,35)}$=2.668, P>0.05]. However, there was a significant interaction between the APP transgene and CS deficiency (P<0.05). *P< 0.05 (*post hoc* test). *B*) Neprilysin immunoreactivity in the hippocampus, excluding the dentate gyrus and the stratum lacunosum-moleculare (CA1–CA3), of 3-mo-old APP-Tg (n=10) and CS-KO/APP-Tg (n=6) mice. **P < 0.01 (Student's t test). *C, D*) Representative hippocampal sections, from APP-Tg (*C*) and CS-KO/APP-Tg (*D*) mice, immunostained with the anti-neprilysin antibody, 56C6. Attenuation of the signal was noted in the pyramidal layer of CA1 and CA2 and in the mossy fibers (arrowheads). Scale bar = 300 μm. Error bars = SE.

ity changes in APP-Tg mice with an increase in CS. In addition, it should be noted that the calpain inhibitors used in most of the previous *in vitro* studies not only target calpain but also block other cysteine proteases, including cathepsins B, H, L, K, and S to a similar extent. A typical example is MDL2817 (43). Our data also suggest that neprilysin expression at presynaptic terminals is disturbed by calpain overactivation. This occurred as early as 2 mo of age in CS-KO/APP-Tg mice and may gradually accelerate Aβ depositions toward the onset of senile plaque formation at around 9 mo of age. It remains to be determined how calpains alter the subcellular localization and/or Aβ-degrading activity of neprilysin; however, direct cleavage or indirect phosphorylation of neurofilaments and microtubule-associated proteins by calpains may cause cytoskeletal disorganization, as outlined below, resulting in retarded axonal transport of neprilysin to the presynaptic compartment. The level of presynaptic neprilysin was elevated after the appearance of Aβ plaques (>12 mo), presumably due to aberrant hypertrophic swelling of presynaptic terminals in the proximity of plaques, and this enhancement could account for the diminished effects of CS deficiency on Aβ deposition in APP-Tg mice from 18 to 26 mo of age as assessed by [^{11}C]PIB-PET. It is also worth noting that augmentation of calpain-10 and its cleavage of SNAP-25 are likely to promote vesicular exocytosis (44) and thus may contribute to the release of Aβ into the extracellular matrix, similar to the regulatory mechanisms by which insulin is secreted from pancreatic β-cells (45, 46). This could add calpains to the components critically implicated in the regulation of Aβ release by synaptic excitation (47, 48).

In addition to its aggressive involvement in Aβ neurotoxicity, calpain could represent a key link between Aβ and tau pathologies in neurodegenerative amyloidosis. This notion is supported by our observation that calpain-10 is pronouncedly up-regulated in APP-Tg plaques and that it colocalizes with somatic and neuritic tau pathologies in AD brains. The toxic properties of tau may result from its limited proteolysis as mediated by calpain (49). The increased level of potentially cytotoxic phospho-tau generated by overactivation of Cdk5 (18, 50, 51) provides another possible mechanism and could account for the development of AT8-positive granular lesions in the hippocampal subiculum of our APP-Tg mice. Disruption of the axonal cytoskeleton also leads to the accumulation of microtubule-unbound tau, which is prone to phosphorylation (18, 52). In addition, activation of the extracellular signal-regulated kinase (Erk) and 1,2-mitogen-activated protein kinase (MAPK) system by calpain (53) may account for the hyperphosphorylation of tau in the absence of CS. Since the Erk-MAPK pathway also mediates tau-induced, NMDA receptor-dependent neurotoxicity (54), calpain conceivably acts as a link between pathogenic tau accumulation and neuronal death by modulating this pathway. It remains to be determined whether activation of Erk-MAPK signaling is critical in the nonapoptotic mechanisms of cellular damage observed in the present study. Although tau abnormalities in APP-Tg mice are secondary to Aβ pathogenesis and calpain up-regulation, they might precede pathologically defined Aβ plaque formation. Given that calpain activation is inducible by soluble Aβ (39), such initial forms of Aβ assembly could consequently impair cytoskeletal frameworks in neurons, as evidenced by dystro-

according to the percentage of injected dose of radioligand per unit tissue volume (%ID/ml). *Q*) Longitudinal changes in amyloid load in the hippocampus of WT (open circles), APP-Tg (open squares), and CS-KO/APP-Tg (solid squares) mice quantified as BP_{ND} for [^{11}C]PIB (n=4/group). *R–W*) Double-immunofluorescence staining with 4G8 (*R, U*) and anti-mouse CS antibody (*S, V*) for neocortical sections of APP-Tg (*R–T*) and CS-KO/APP-Tg (*U–W*) mice. Two-channel photomicrographs demonstrate intense labeling for CS in the proximity of amyloid plaques in the APP-Tg mice (*T*). This is completely abolished in CS-KO/APP-Tg mice (*W*). *P< 0.05 (Fisher's least-square difference *post hoc* test following 2-way ANOVA); †P< 0.05 (t test). Error bars = SE. Scale bars = 1 mm (*A–C, I–K*); 50 μm (*E–G*); 25 μm (*R–W*).